A&A manuscript no.
(will be inserted by hand later)

Your thesaurus codes are:
08(02.01.3; 02.12.1; 08.01.1; 08.05.1; 08.19.3)

ASTRONOMY
AND
ASTROPHYSICS
May 28, 2000

Non-LTE line formation for neutral oxygen

Model atom and first results on A-type stars ⋆

N. Przybilla[1,2], K. Butler[1], S.R. Becker[1], R.P. Kudritzki[1,2,3], and K.A. Venn[4]

[1] Universitäts-Sternwarte München, Scheinerstraße 1, D-81679 München, Germany
[2] Max-Planck-Institut für Astrophysik, Karl-Schwarzschild-Straße 1, D-85740 Garching bei München, Germany
[3] University of Arizona, Steward Observatory, 933 N. Cherry Av., Tucson AZ 85721, USA
[4] Macalester College, Department of Physics and Astronomy, 1600 Grand Ave., St. Paul, MN 55105, USA

Received / Accepted

Abstract. An extensive model atom for non-LTE line formation calculations for O I is presented, taking into account recent improvements in the atomic data. Based on line-blanketed LTE model atmospheres equivalent widths are computed in LTE and non-LTE for the diagnostic O I lines of A- and late B-type stars in the range $T_{\rm eff} = 7500$ K to 15000 K and luminosity classes V to Ia. Non-LTE abundance corrections are provided: they span a wide range in magnitude, from less than 0.1 dex for the weak lines in main sequence stars to more than 1.5 dex for the near-infrared lines in some supergiants.

The dependence of the non-LTE effects on the atmospheric parameters is discussed with special emphasis on supergiants. In particular, the near-infrared transitions are found to react sensitively to the collisional excitation cross sections used in the calculations. Further investigations concentrate on the influence of microturbulence and on the rôle of wind outflow velocity fields on the line formation.

As a test and first application of the model, oxygen abundances for Vega (A0 V), η Leo (A0 Ib) and HD 92207 (A0 Iae) are derived. The analysis of Vega confirms a slight oxygen underabundance ($\sim$0.3 dex) in this star while η Leo and HD 92207 show a nearly solar value. For Vega the observed spectrum can be reproduced accurately by the calculated line profiles. In supergiants consistent abundances can be derived from the weak lines in the visible. At high luminosities the prominent near-infrared features – among other strong lines from different elemental species – are subject to additional broadening by an unidentified process which prevents an equally accurate theoretical interpretation.

Key words: Atomic data – Line: formation – Stars: abundances, early-type, supergiants

Send offprint requests to: N. Przybilla (nob@usm.uni-muenchen.de)

⋆ Based on observations collected at the European Southern Observatory, Chile (ESO N° 62.H-0176)

1. Introduction

Oxygen is the most abundant metal and therefore of primary interest in cosmochemical studies. Abundance determinations at extragalactical distances have been restricted to studies of H II regions (see e.g. Skillman 1998) until recently. The generation of large telescopes presently coming into operation and their dedicated spectrographs now provide the tools for quantitative spectroscopy of luminous stars at distances as far as the Virgo and Fornax clusters (Kudritzki 1998, Kudritzki et al. 1999). Primary targets for ground based observations of extragalactic stars are A- & B-type supergiants as they appear brightest in the visual.

Being young stars, these supergiants reflect the present composition of the surrounding interstellar medium, offering an independent method for deriving abundances in addition to H II region studies. At the same time they are evolved objects with CNO-cycled gas mixed into the atmosphere. Furthermore, they are the progenitors of type II supernovae, the main contributors to the enrichment of the ISM with oxygen. Abundance analyses of supergiants are therefore of importance for the verification of evolutionary scenarios of massive stars (see Venn (1995a) for results on galactic A-type supergiants) as well as for the chemical evolution of galaxies.

For oxygen, reliable abundance determinations for supergiants are scarce. Previous analyses of late B- and A-type stars (abbreviated as BA-type stars) are mainly based on either LTE calculations or on rather simple non-LTE model atoms. Pioneering work on non-LTE effects for neutral oxygen was performed by Baschek et al. (1977) and the contributions so far culminated in a comprehensive model atom published by Takeda (1992). In the meantime, improved line-blanketed model atmospheres have become available (Kurucz 1991) and the accuracy of atomic data has been enhanced enormously due to the efforts of e.g. the Opacity Project (OP; see Seaton et al. (1994) for a general overview). A critical reinvestigation seems appropriate as abundances derived from different spectral lines are inconsistent. The point of interest will be the weak lines in the visible and the strong features in the near-infrared, especially the $\lambda\lambda$ 7771-5 triplet which is a powerful luminosity criterion and most prominent in supergiants (Faraggiana et al. 1988).

At lower temperatures, in the F and G stars, these triplet lines also have a long history as controversial abundance indicators when compared to other oxygen features. Starting with the work of Johnson et al. (1974) non-LTE effects have been discussed by a number of authors, see e.g. Kiselman (1993), Cavallo et al. (1997) or Reetz (1998) for recent results. Despite many promising approaches to the topic a comprehensive theoretical interpretation of the observations is still lacking.

Kudritzki (1992) first investigated the effects of a transsonic velocity field (i.e. the stellar wind) on the formation of weak ("pseudophotospheric") metal lines. Later, Lamers & Achmad (1994) concluded that the apparent high microturbulence velocities derived for A and F supergiants are due to mass loss. The O I spectrum in A-type supergiants (with both weak and extremely strong features) offers an excellent opportunity for verifying the predictions as these stars are slow rotators as compared to those of earlier spectral type where large rotation velocities are likely to mask the mass loss effects.

In this paper we present the basics for an accurate abundance determination of neutral oxygen in BA-type stars with special emphasis on supergiants. A comprehensive model atom for O I is presented in the next section together with a critical examination of the expected uncertainties. The results from our LTE and non-LTE line formation computations are described in Sect. 3 while in the following section a test sample of high S/N and high resolution spectra of three stars is analysed for oxygen abundances. In Sect. 5 we discuss the impact of micro- and macroscopic velocity fields on the line formation. Finally, a short summary is given.

The application of the model to the determination of oxygen abundances in extragalactic supergiants (see Przybilla et al. (1999) for first results) and the implications for galactic abundance gradients will be the subject of further investigation when a sufficiently large sample of observations becomes available.

2. Model calculations

2.1. Model atmospheres and programs

The calculations are performed using the standard assumptions of plane-parallel, homogeneous and stationary stellar atmospheres in hydrostatic and radiative equilibrium. Oxygen, although the most abundant metal, is supposed to be a trace element. The photoionization edge of the O I ground state coincides with the Lyman edge and the resonance lines fall into the same wavelength range as the Lyman series, thus contributing only a small fraction to the dominating hydrogen opacity; changes in the oxygen populations therefore have no appreciable effects on the atmospheric structure. Thus we obtain statistical equilibrium populations for O I while keeping the run of the atmospheric parameters fixed.

The non-LTE O I line profiles are computed on the basis of ATLAS9 (Kurucz 1979, 1991) LTE line-blanketed model atmospheres using LTE Opacity Distribution Functions (Kurucz 1992) to account for line blocking in the spectrum synthesis. For the calculation of model atmospheres for the most extreme supergiants close to the Eddington limit, modifications in the treatment of opacities and the radiative pressure in the outermost depth points within ATLAS9 have been made to achieve convergence. Comparisons at stellar parameters for which standard ATLAS9 converges have shown that the stratification deeper in the atmosphere is only marginally affected by these modifications.

With the assumptions cited above reliable analyses can be performed in the given temperature range from main sequence stars through to bright giants as indicated by Kudritzki (1988). Late A-type stars are an exception since an outer convection zone may be of importance as the observation of chromospheres in these stars proves, see Simon & Landsman (1997) for the latest discoveries. Convection is therefore taken into account in the standard way for ATLAS9 atmospheric models with $T_{\rm eff} < 8500\,{\rm K}$ applying a value $\ell/h = 1.5$ of mixing length to scale height.

A thorough discussion of the possible deviations from the standard assumptions on the model atmosphere structure of supergiants is given by Venn (1995b). Additionally, non-LTE effects are often less significant on the model structure than line blanketing as demonstrated by Przybilla (1997).

The line formation calculations are performed using the programs DETAIL and SURFACE (Giddings 1981, Butler & Giddings 1985), with the former solving the radiative transfer and the statistical equilibrium equations and the latter computing the emergent flux. Recent improvement by inclusion of an ALI scheme (using the treatment of Rybicki & Hummer 1991) allows the utilisation of quite elaborate model atoms while the necessary computational resources remain at a low level. Optionally, effects of wind outflow velocity fields can be studied by adopting the ALI operator in the comoving frame as described by Puls (1991). Unified model atmospheres accounting for spherical extension and stellar wind but lacking line blanketing (Santolaya-Rey et al. 1997, SPH) replace the ATLAS9 atmospheres in the latter case.

2.2. The model atom

2.2.1. Energy levels

Neutral oxygen lines are most prominent in late A-/early F-type stars where the population of the excited energy levels reaches its maximum. At higher temperatures within our parameter range oxygen becomes rapidly ionized but only a negligible population is expected for excited O II energy levels connected to the ground state via radiatively permitted transitions as high excitation energies ($\gtrsim$ 15 eV) are involved. It is therefore sufficient to take only the ground state of O II into account.

Since the O I lines in the visible originate from excited levels ($\gtrsim$ 9 eV above the ground state), the O I model atom has to be fairly complete with respect to these levels. All energy levels below an excitation energy of 13.4 eV as listed by Moore

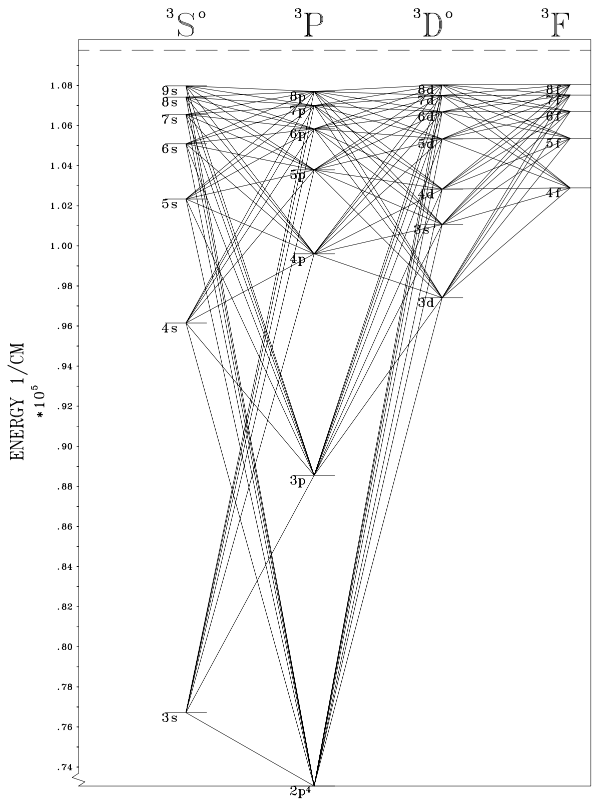

Fig. 1. Grotrian diagram for the O I triplet system.

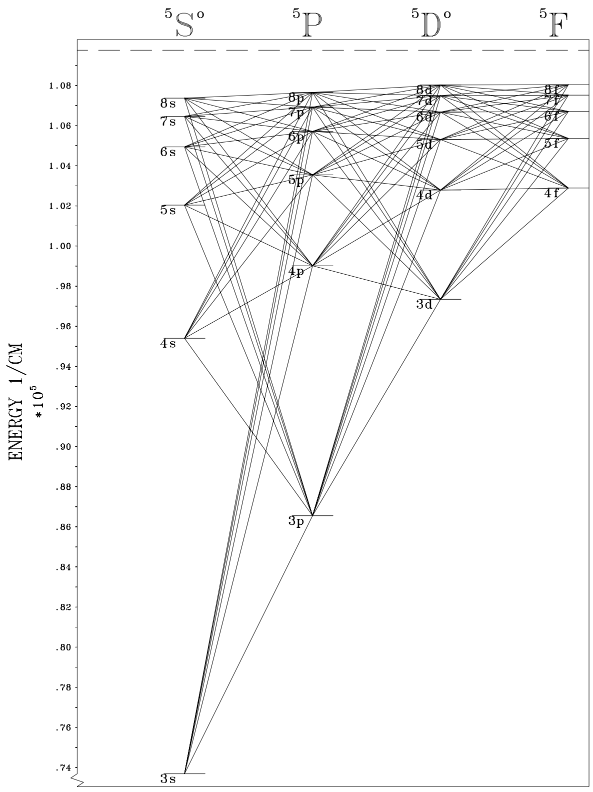

Fig. 2. Grotrian diagram for the O I quintet system.

(1976) are included explicitly in the model atom, together with additional P terms for principal quantum number $n = 7$, 8 and F terms for $n = 8$, adopted from OP computations (Butler & Zeippen, 2000). Sub-levels belonging to the same term are combined into a single level.

Additionally, level populations of O I up to $n = 10$ are computed in LTE relative to the ground state of O II with energies derived from their quantum defects. They are considered only in the number conservation equation.

2.2.2. Radiative transitions

All optically allowed bound-bound transitions between energy levels with non-LTE populations are taken into consideration. The required LS-coupling oscillator strengths are adopted from OP data (Butler & Zeippen, 1991, 2000). The reduction of individual lines of a multiplet into a single effective line introduces only small errors in the transition rates and occupation numbers as Baschek et al. (1977) have shown. In order to improve the computational efficiency we therefore ignore fine-structure splitting.

Grotrian diagrams of the triplet and quintet spin systems are shown in Fig. 1 and Fig. 2. Both spin systems together with the singlets ($2p^4\ ^1D$, $2p^4\ ^1S$, $2p^3(^2D^o)3s\ ^1D^o$) are treated simultaneously, the latter couple to the triplets via intercombination and forbidden transitions. The only direct coupling between the triplets and quintets is provided by the intersystem line λ 1356 ($2p^4\ ^3P$ – $3s\ ^5S^o$); oscillator strengths for the latter transitions are taken from the compilation of Wiese et al. (1996). A detailed comparison of the adopted oscillator strengths with measurements and theoretical work by other authors is performed by Butler & Zeippen (1991); the majority of the data is expected to be accurate to within 10% outdating most of the older data used in previous studies of non-LTE effects on O I.

Photoionizations from all energy levels with non-LTE populations are treated with cross sections fitted to the OP data (Butler & Zeippen, 1990, 2000). A carefully chosen frequency grid ensures a thorough representation of the numerous resonances present in the results of R-matrix calculations. Butler & Zeippen (1990) discuss the reliability of the cross sections for the first three states of O I in the context of the available experimental data and theoretical results from the literature; excellent agreement was found. The expected accuracy of the bulk of the OP photoionization cross sections amounts to approx. $\pm 10\%$.

A comparison of photoionization cross sections for the ground state and the quintet metastable state is presented in Fig. 3. Discrepancies up to an order of magnitude at threshold are present between the OP calculations and the data of Hofsäß (1970) used in the O I study of Baschek et al. (1977).

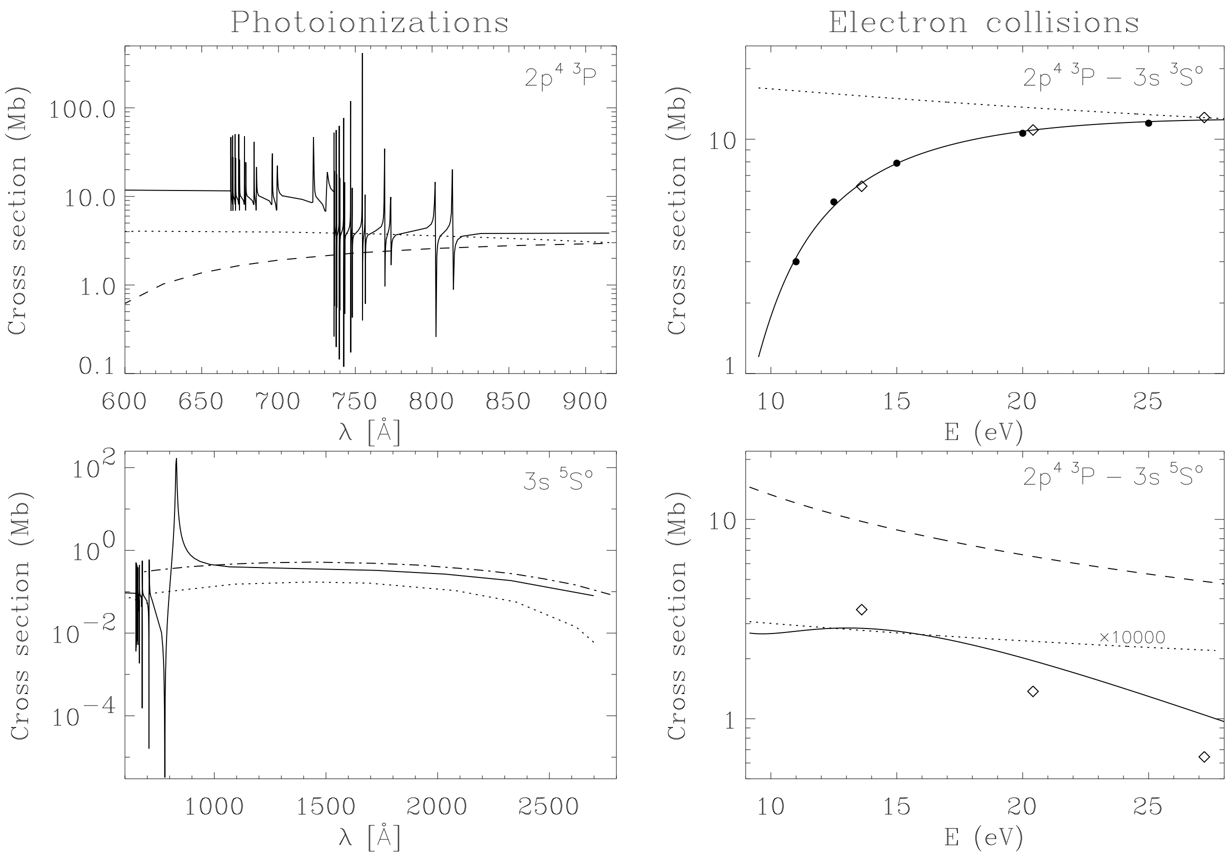

Fig. 3. Comparison of different photoionization cross sections (left panel) and excitation cross sections for electron collisions (right panel) on a logarithmic scale. Displayed are cross sections from OP computations (full line) and data from Hofsäß (1970, dotted), Henry (1970, dashed) and Peach (1967, dashed-dotted) for the photoionizations. In the case of the electron collisions our analytical fit (full line in upper diagram) to measured cross sections (Wang & McConkey, 1992, dots) is shown, as well as results from the approximations from Van Regemorter (1962, dotted) and from Allen (1973, dashed) and the theoretical data of Tayal & Henry (1989, full line in lower diagram) and Sawada & Ganas (1973, diamonds). Note that the Van Regemorter results are multiplied by a factor of 10000 in the lower right diagram.

Takeda (1992) uses cross sections provided by Henry (1970) and calculated according to Peach (1967). These are in better agreement with the OP data but for the cross sections of levels at higher energies he uses the hydrogenic approximation which provides reasonable results only for high quantum numbers ℓ. In summary, the use of the OP data significantly improves the description of the photoionization processes compared to previous O I non-LTE studies.

In the first step of the computations, i.e. in DETAIL, the level populations are calculated using depth dependent Doppler profiles assuming LS coupling; microturbulence is explicitly accounted for by inclusion of an additional term in the Doppler width ($\Delta\lambda_{\rm D}$):

$$\Delta\lambda_{\rm D} = \frac{\lambda_0}{c}\sqrt{v_{\rm th}^2 + \xi^2} \tag{1}$$

where λ_0 is the rest wavelength of the transition, c the speed of light, $v_{\rm th}$ the thermal velocity for the chemical species of interest and ξ the microturbulent velocity; see Sect. 5 for a discussion. Both continuous opacities and ATLAS9 line-distribution functions are accounted for in solving the radiation transfer.

These LS-coupling populations are then split according to the statistical weights of the individual sub-levels in order to calculate line profiles via the program SURFACE; Voigt profile functions are adopted and the same microturbulent velocity as in DETAIL is applied. The damping parameters are calculated from radiative lifetimes given by Butler & Zeippen (2000) for the radiative widths and from the approximation of Cowley (1971) for collisional damping. A comparison with profiles computed with the more sophisticated data from Griem (1974) shows only negligible differences.

2.2.3. Collisional transitions

Special attention should be paid to an accurate description of electron collisions in view of their importance for the balance between the different spin system populations. Energy-resolved measurements for only a few transitions from the ground state are found in the literature; the results of Wang & McConkey (1992) are adopted. Theoretical cross sections for collisions between the ground state and the low excited singlet

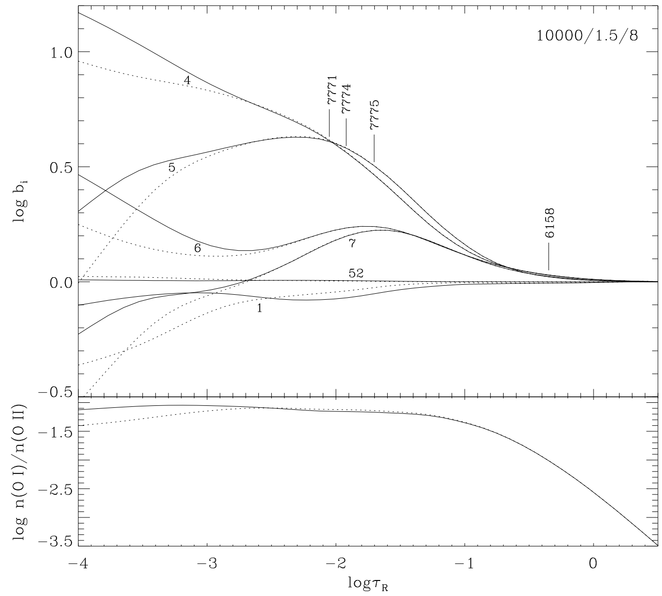

Fig. 4. Effects of the charge exchange reaction $\mathrm{O}^0\,(2\mathrm{p}^4\ ^3\mathrm{P}) + \mathrm{H}^+ \rightleftharpoons \mathrm{O}^+\,(2\mathrm{p}^3\ ^4\mathrm{S}^o) + \mathrm{H}^0\,(1\mathrm{s}\ ^2\mathrm{S})$ on the departure coefficients and the ionization balance of oxygen as function of the Rosseland optical depth τ_R in a supergiant model for T_eff=10000 K, log g=1.5, ξ=8 km s^{-1}. Solid line: with, dotted line: without charge exchange. The formation depths of the line core ($\tau \approx 1$) for several transitions are indicated. Term identifiers – 1: $2\mathrm{p}^4\ ^3\mathrm{P}$; 4: $3\mathrm{s}\ ^5\mathrm{S}^o$; 5: $3\mathrm{s}\ ^3\mathrm{S}^o$; 6: $3\mathrm{p}\ ^5\mathrm{P}$; 7: $3\mathrm{p}\ ^3\mathrm{P}$; 52: $2\mathrm{p}^3\ ^4\mathrm{S}^o$ (O II)

levels are taken from Tayal (1992). Results for the transitions to quintet terms were calculated by Tayal & Henry (1989) together with some additional cross sections in the triplet spin system. From a comparison with data presented in former work an accuracy significantly better than a factor of 2 is expected. For all remaining transitions up to the $3d$ energy levels the collision strengths from the distorted wave calculations of Bhatia & Kastner (1995) are used. The authors claim a generally good accuracy, even in the worst case being better than an order of magnitude, despite the fact that this method is not well suited for neutral species. For all other optically allowed transitions the Van Regemorter formula (Van Regemorter 1962) is applied with OP oscillator strengths. All the remaining bound-bound transitions are treated according to the semiempirical Allen formula (Allen 1973) with the collision strength Ω set equal to 1.0.

In Fig. 3 the collisional cross sections used in this work are compared to those derived from the approximation formula of Van Regemorter (1962) as adopted by Baschek et al. (1977). Large discrepancies up to several orders of magnitude are found. For the optically forbidden transition the cross section according to Allen (1973) and the results from the distorted-wave calculations of Sawada & Ganas (1973) as used by Takeda (1992) are also displayed. The former offers a better description than the Van Regemorter approximation; the latter are in good agreement with the data preferred by us. In summary, the preference of experimental and sophisticated theoretical data over results from approximation formula for many important transitions improves the reliability of our statistical equilibrium calculations.

Experimental cross sections from Thompson et al. (1995) are adopted for the collisional ionization of the ground state. Agreement better than a factor of 2 within the measured energy range is expected confirming previous results from other authors. Supplementary cross sections for ionization from $n = 3$ triplet levels are provided by Chung et al. (1993). Their comparison for different theoretical approaches suggests an accuracy better than 50%. The Seaton formula (Seaton 1962) is used for collisional ionization of the remaining non-LTE levels; threshold photoionization cross sections are taken from the OP data.

2.2.4. Charge exchange reactions

The nearly resonant charge exchange reaction $\mathrm{O}^0\,(2\mathrm{p}^4\ ^3\mathrm{P}) + \mathrm{H}^+ \rightleftharpoons \mathrm{O}^+\,(2\mathrm{p}^3\ ^4\mathrm{S}^o) + \mathrm{H}^0\,(1\mathrm{s}\ ^2\mathrm{S})$ has been taken into account in the non-LTE calculations with rate coefficients determined according to the analytic fits of Arnaud & Rothenflug (1985). Non-LTE level populations n_i of hydrogen are calculated with DETAIL on the ATLAS9 model structure in advance. They show departure coefficients b_i=$n_i^\mathrm{NLTE}/n_i^\mathrm{LTE}$ differing significantly from unity only close to the Eddington limit (Kudritzki 1973). This process dominates the ionization balance of oxygen as the departures of the n(H I $1\mathrm{s}\ ^2\mathrm{S}$)/$n$(H II) ratio are forced upon n(O I $2\mathrm{p}^4\ ^3\mathrm{P}$)/$n$(O II $2\mathrm{p}^3\ ^4\mathrm{S}^o$) – and the first two low-lying terms $2\mathrm{p}^4\ ^1\mathrm{D}$ and $2\mathrm{p}^4\ ^1\mathrm{S}$ which are in detailed balance with the O I ground state. Note that the O I/II ground states are already thermalized throughout most of the atmosphere when the charge exchange reaction is neglected (Fig. 4). As a consequence, the formation depths for the spectral lines discussed here are only marginally affected by charge exchange even for supergiants, resulting in negligible effects on the line strengths as tests have shown. Small effects on the W_λ are expected for the resonance lines in the UV only.

For the case of spherically extended unified model atmospheres with strong winds (cf. Santolaya-Rey et al. 1997) significant non-LTE departures for hydrogen are present even in the line formation layers. But again, by omitting the charge exchange reaction negligible effects on the strengths of O I lines originating from the excited levels are found. Strong effects on the departure coefficients can only be expected beyond the sonic point.

2.3. Error estimates for the oxygen non-LTE calculations

To assess the importance of various parameters entering the non-LTE computations and to estimate systematic errors on the abundance analysis test calculations are performed for typical supergiant atmospheric parameters in the given temperature range: $T_\mathrm{eff}/\log g$ of 8500 K/1.0, 10000 K/1.5 and 15000 K/2.0 with the microturbulence fixed at $\xi = 8\,\mathrm{km\,s^{-1}}$ assuming solar metallicity. Below $T_\mathrm{eff}\approx$8500 K the hydrostatical model atmospheres for supergiants develop pressure inversion and should therefore – as well as for other reasons – be viewed with cau-

Table 1. Uncertainties in the non-LTE analysis of O I

	changes in $\log\varepsilon(\mathrm{O})_{\mathrm{NLTE}}$		
	8500/1.0	10000/1.5	15000/2.0
Atmospheric parameters:			
$T_{\mathrm{eff}}\ -150\,\mathrm{K}$	-0.09	-0.04	-0.02
$\log g\ +0.15$	-0.09	-0.05	-0.06
$\xi + 1\,\mathrm{km\,s^{-1}}$ [a]	-0.05	-0.01	± 0.00
Line transitions:			
Oscillator strengths $+10\%$	-0.06	-0.06	-0.05
Damping constant $*0.5$, $*2$	± 0.00	± 0.00	± 0.00
Photoionizations:			
Cross-sections $+10\%$	± 0.00	± 0.00	± 0.00
Cross-sections $*5$	$+0.17$	$+0.23$	$+0.30$
Collisional transitions[b]:			
Cross-sections $*0.1$	-0.05	-0.05	-0.06
Cross-sections $*0.5$	-0.02	-0.03	-0.03
Cross-sections $*2$	$+0.04$	$+0.03$	$+0.04$
Cross-sections $*10$	$+0.14$	$+0.14$	$+0.17$
Collisional ionization:			
Cross-sections $*0.1$, $*10$	± 0.00	± 0.00	± 0.00
Charge exchange reaction:			
Rate coefficients $*0.1$, $*10$	± 0.00	± 0.00	± 0.00
Continuum placement	± 0.05	± 0.05	± 0.05
Estimated total uncertainty	± 0.16	± 0.11	± 0.10

[a]: mean values without the near-infrared transitions
[b]: mean values without the near-infrared transitions which can show deviations >0.5 dex at a factor 10

tion as a reliable description of the physical conditions. For a given synthetic spectrum of O I the abundance is adjusted in the model with modified parameters to reproduce the original line strengths. The results of the tests (mean values from the analysed lines) are summarised in Table 1.

Uncertainties in the atmospheric parameters (at typical values of our analyses) have the largest effects on the non-LTE abundance determination for oxygen. Here one has to rely on the weak lines in the visible as the strong near-infrared lines react sensitively to even small changes in the microturbulent velocity. In any case, these lines are abundance indicators of only limited reliability for reasons discussed below.

Errors in the abundances derived from weak lines are directly proportional to inaccuracies in the gf values. The 10% overall error anticipated from the OP data manifests itself in an abundance uncertainty of ∼0.05 dex. Nevertheless, this might be an underestimate for individual transitions, cf. Table 4.

Generally, uncertainties in the line broadening due to radiative lifetimes are negligible. In the case of collision broadening the comparison of our values with Stark-broadening parameters from Griem (1974) for selected lines results in almost identical line profiles. But it should be noted that a typical error of a factor 2 in the collisional damping half-widths mainly affects the strong near-infrared lines.

No systematic error on the abundance analysis is expected from the variation of OP photoionization cross-sections within the given error bars. A factor of 5 in the absolute values of the cross-sections – a difference easily reached in comparison with former studies – on the other hand results in significant abundance corrections. The near-infrared lines are most strongly affected. But even this is an underestimation, larger differences are present even in some of the threshold values, amounting to factors of 10^2-10^3 in the – sometimes broad – resonances. The use of the OP data certainly results in a significant improvement compared to former O I studies.

Collisional excitation cross-sections also prove to be critical parameters in our statistical equilibrium computations. Unfortunately, for most of the transitions the data are based on an approximate formula, giving an accuracy within a factor 2 or 3 at best near threshold. Nevertheless, we do not expect larger overall systematic errors for our model than given in the corresponding entry of Table 1 as for the most important transitions quite accurate data are used. In-/decreasing the cross-sections by a factor 10 and therefore shifting farther to/from LTE conditions results in comparatively large abundance uncertainties and demonstrates again the need for accurate atomic data. The importance of detailed collisional data for the development of the strong non-LTE effect in the near-infrared triplet will be discussed later.

It is found that the accuracy of the collisional ionization cross sections is not a critical factor in the non-LTE computations as scaling them by a factor as large as 10 has virtually no effect on the calculated equivalent widths. Due to the small mean kinetic energy of the colliding electrons the low lying levels are not depopulated and thus the ionization balance is only marginally affected.

Inaccuracies in the rate coefficients of the charge exchange reaction have no effect on the abundance analysis in our approach as the changes occur only outside the line forming region.

Another source of systematic error is the continuum placement in the observed spectra. This strongly depends on the S/N ratio obtained. Our estimate in Table 1 should be applicable to high quality data with S/N>150 only. In general, equivalent widths studies are more susceptible to this systematic error than the spectrum synthesis technique which also accounts for the continuum regions.

The total uncertainties are computed from the sum of the squares of the appropriate uncertainties listed above. They should be viewed as the systematic errors applicable to our non-LTE calculations on O I *within* our methodology (cf. Sect. 2.1).

For our model of the supergiant HD 92207 (see Sect. 4) we performed the same parameter study as above to examine the reliability of our abundance analysis *close* to the Eddington limit. We find an estimated total uncertainty of ± 0.13 dex with errors due to the atmospheric/atomic parameters similar to those from Table 1. Note that the uncertainties in the atmospheric parameters of this star might be larger than adopted here thus increasing the systematic error. Finally, for main sequence stars we expect slightly smaller systematical errors than from Table 1 as most of the observed lines are formed under LTE conditions, the detailed atomic structure becoming irrel-

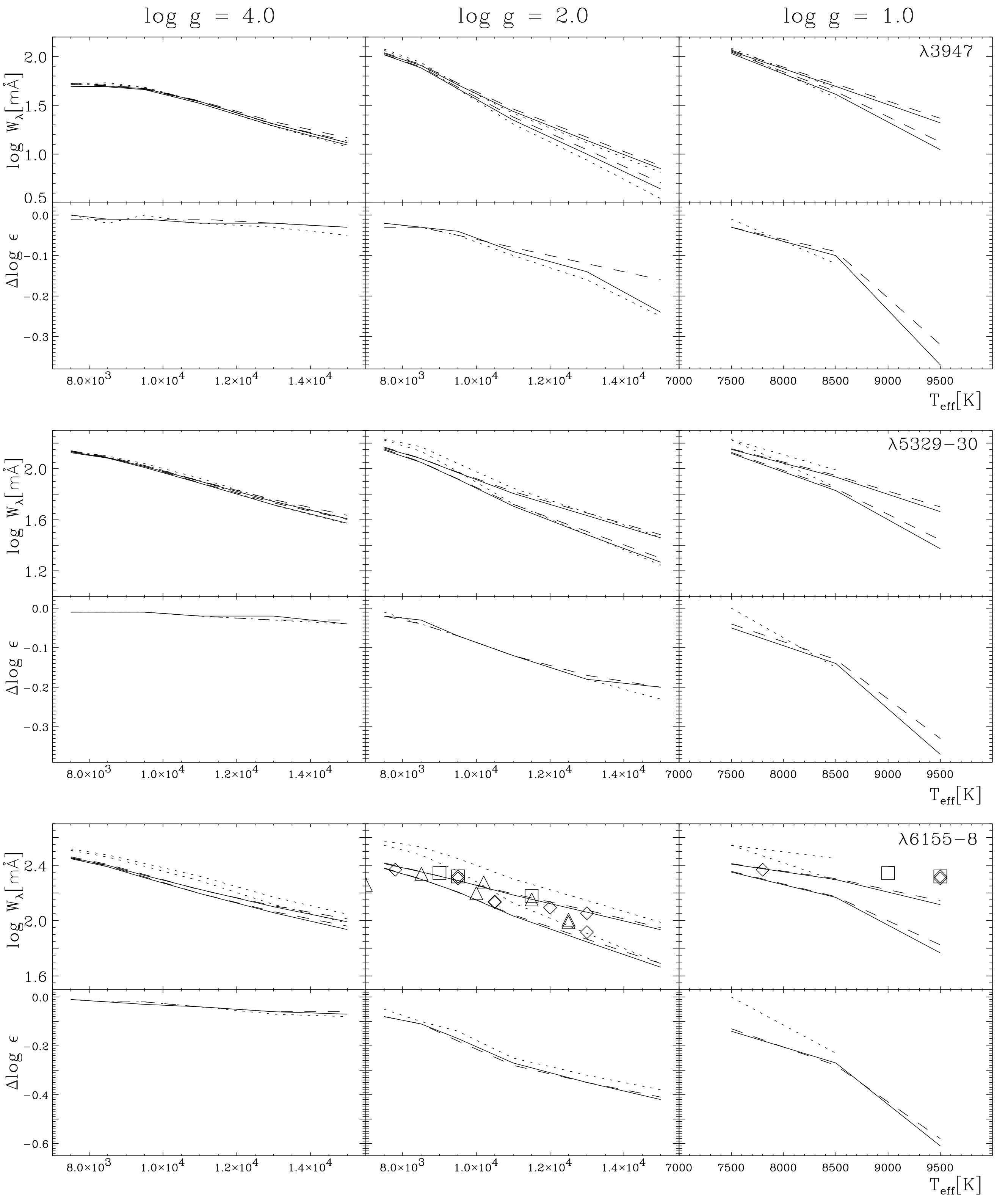

Fig. 5. Theoretical equivalent widths W_λ (in mÅ) and non-LTE corrections $\Delta\log\varepsilon$ (as defined by Eq. 3) as a function of $T_{\rm eff}$ for values of $\log g$ suitable for stars of luminosity class V, Ib and Ia. Solid line: $\xi = 2\,{\rm km\,s^{-1}}$, [O/H] $= 0$, [Fe/H] $= 0$; dotted line: $\xi = 8\,{\rm km\,s^{-1}}$, [O/H] $= 0$, [Fe/H] $= 0$; dashed line: $\xi = 2\,{\rm km\,s^{-1}}$, [O/H] $= 0$, [Fe/H] $= -0.7$. The non-LTE equivalent widths are larger than their LTE counterparts. Note the different temperature range for the Ia results. For $\lambda\lambda$ 6155-8 observed W_λ according to Takeda & Takada-Hidai (1998) are also displayed. Triangles, squares, diamonds: Ib, Iab, Ia supergiants.

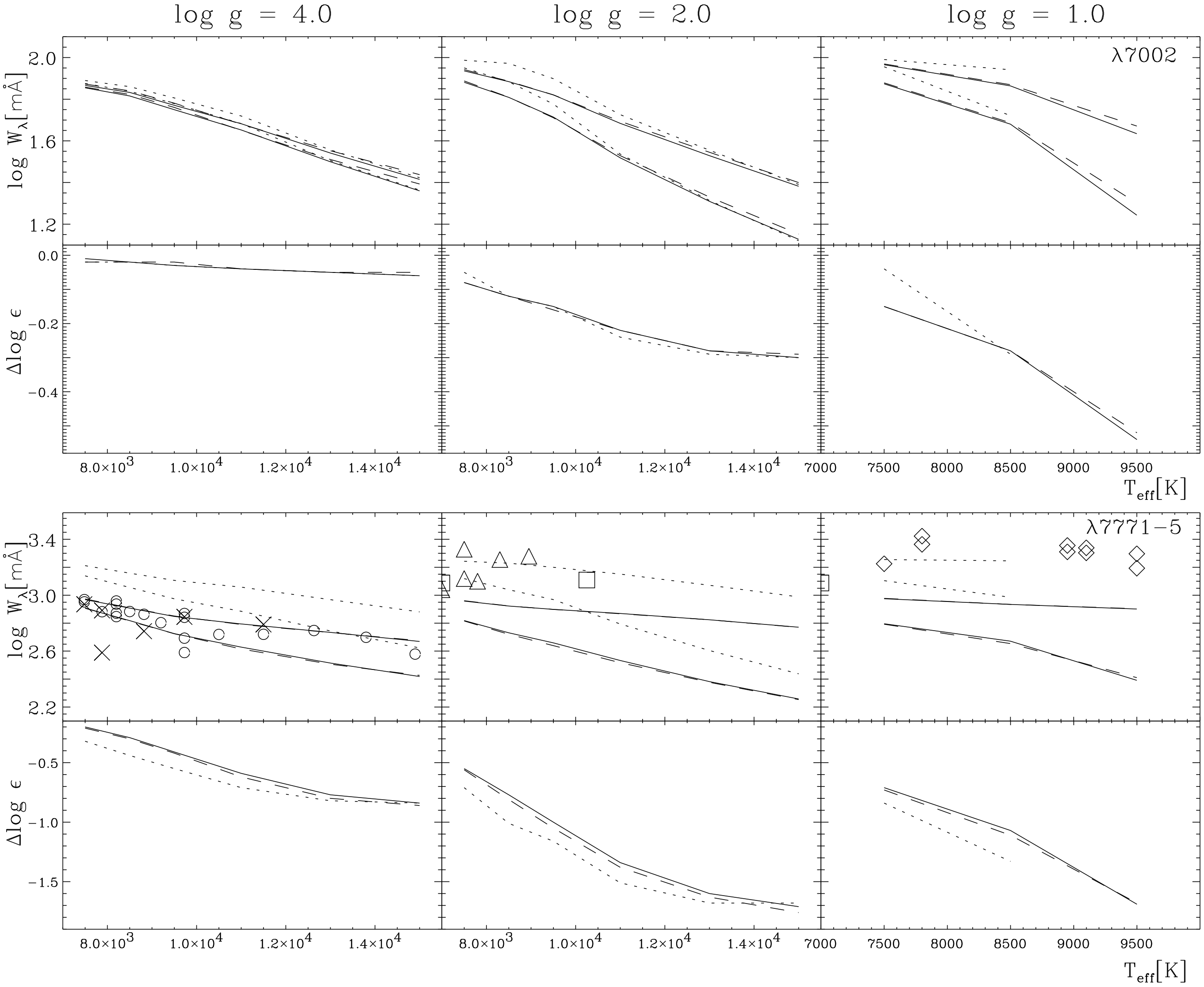

Fig. 5. (cont.). For the near-infrared triplet $\lambda\lambda$ 7771-5 observed W_λ according to Faraggiana et al. (1988) are also displayed. Circles: main sequence stars; crosses: subgiants; triangles, squares, diamonds: Ib, Iab, Ia supergiants.

evant. The given uncertainties should therefore be viewed as upper limits for objects on the main sequence. In particular, for Vega (see Sect. 4) we derive a total uncertainty of $\pm$0.08 dex from the parameter study.

3. Discussion

In this section we evaluate the advantages of time consuming non-LTE calculations over a straightforward LTE analysis for the interpretation of the O I spectra of BA-type stars. First, we present the results of our model calculations in the form of a grid of equivalent widths and non-LTE corrections for a set of diagnostic O I lines applicable to abundance studies. In the following the nature of the non-LTE effects is discussed for the parameter space of BA-type stars. The problems with modelling the observed strong near-infrared lines are addressed and finally our results are compared with those of previous studies of non-LTE effects in atomic oxygen.

3.1. Results of our model calculations

Fig. 5 summarises our results on the O I lines $\lambda\lambda$ 3947, 5329-30, 6155-8, 7002 and 7771-5. Displayed are the computed equivalent widths W_λ from LTE and non-LTE calculations summed over all components of a transition for a given oxygen abundance

$$\log\varepsilon = \log(N_{\rm O}/N_{\rm H}) + 12 \quad (2)$$

and expected non-LTE abundance corrections

$$\Delta\log\varepsilon = \log\varepsilon_{\rm NLTE} - \log\varepsilon_{\rm LTE} \quad (3)$$

as a function of $T_{\rm eff}$ for surface gravities typical for main sequence stars, Ib and Ia supergiants. The $\Delta\log\varepsilon$ are calculated

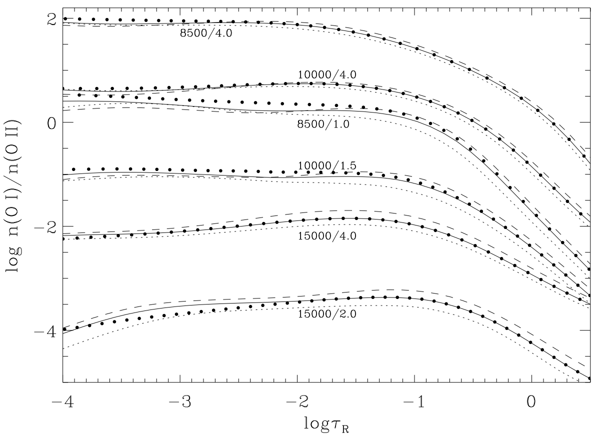

Fig. 6. Ratio of O I to O II non-LTE populations as a function of τ_R for different stellar parameters T_{eff} / $\log g$. The same line identifiers as in Fig. 5 are used. For the $\xi = 2\,\mathrm{km\,s^{-1}}$ model at solar oxygen content and metallicity the LTE ratio is also displayed (thick dots).

from LTE abundances adjusted to reproduce the equivalent widths obtained in the non-LTE computation. In order to account for effects introduced by the variation of other important stellar parameters three sets of calculations were performed, for microturbulences of ξ=2 and 8 km s^{-1} at solar elemental abundances and for ξ=2 km s^{-1} at a composition reduced by 0.7 dex as expected for e.g. SMC objects. The oxygen abundance is kept fixed at the solar value in the latter case. This small inconsistency is acceptable as we are mainly interested in the effects of an increased UV ionization flux on the oxygen ionization balance. A reduced oxygen content will confine the line formation to deeper layers.

Several important conclusions can be drawn from Fig. 5. As expected, the predicted equivalent widths for the BA-type stars decrease monotonically with increasing temperature as oxygen becomes more and more ionized (cf. Fig. 6); at constant T_{eff} the ionization balance is shifted to the higher ionization stage at lower surface gravities but this is overcompensated by an increased population of the excited energy levels, resulting in a strengthening of the lines. Electron collisions become less effective in the low density conditions in supergiants thus favouring departures from LTE. The non-LTE abundance corrections also increase with temperature as deviations from LTE occur in an increasing fraction of the line formation region. In the late A-types only the line centres are affected by non-LTE (see also Sect. 3.1) resulting in small non-LTE corrections.

Non-LTE effects on the weak O I lines in the visible are negligible for main sequence stars but the situation changes markedly in supergiants. For objects close to the Eddington limit non-LTE corrections can amount to $\gtrsim$0.5 dex even for these weak lines. Observed equivalent widths from Takeda & Takada-Hidai (1998) are included in Fig. 5 for O I $\lambda\lambda$ 6155-8 with their effective temperatures adopted. Note that the gravities of these stars span the range $1 \leq \log g \leq 2.3$ thus introducing some of the scatter around our predictions for fixed $\log g$. Moreover, Takeda & Takada-Hidai (1998) also find a reduced iron abundance for most of those stars with significantly smaller $W_\lambda(\lambda\lambda\,6155\text{-}8)$ thus implying a general metal underabundance for these objects.

The near-infrared triplet on the other hand is significantly affected by non-LTE effects even on the main sequence, reaching a dramatic non-LTE strengthening in supergiants. In the case of $\lambda\lambda$ 7771-5 observed equivalent widths from Faraggiana et al. (1988) are also displayed in Fig. 5. Effective temperatures are assigned to spectral types via the relations given by Gray (1992) and Humphreys & McElroy (1984) for main sequence stars and for supergiants, respectively. Good agreement between theory and observation is found in a statistical sense near the main sequence despite the fact that the stellar parameters – and individual oxygen abundances – may differ from our assumed values. For supergiants the discrepancies between theory and observation increase with increasing luminosity. This trend is not due to small number statistics but is a genuine effect as will be shown later.

Microturbulence has no significant influence on the non-LTE abundance corrections apart from its classical effect of strengthening lines on the flat part of the curve of growth. Our (moderate) changes in metallicity also have no strong impact on the $\Delta \log \epsilon$.

The weak lines should be viewed as the spectral features reproduced most convincingly by theoretical means and therefore are to be preferred in abundance analyses. A much greater challenge is posed by the modelling of the observed strong near-infrared lines $\lambda\lambda$ 7771-5 and 8446 in supergiants for which we cannot obtain results consistent with those from the observed weak lines in our simple approach. The discussion of these problems will be resumed later, but we first wish to gain some quantitative insight into the dependence of the non-LTE effects on the model parameters.

3.2. *The non-LTE effects*

The non-LTE ionization balance for oxygen at various stellar parameters is displayed in Fig. 6. At mid-A type temperatures O I is the dominant ionization stage but oxygen rapidly ionizes with increasing T_{eff} and decreasing $\log g$. The variations of the ionization balance with microturbulence and metallicity reflect the changes in the line blanketing at these parameters. In addition, the non-LTE ionization balance for oxygen deviates only marginally from that under LTE conditions as displayed in Fig. 6 for selected cases.

Departure coefficients b_i for the energy levels i are displayed in Fig. 7 as a function of the Rosseland optical depth τ_R for main sequence and supergiant models of mid-/early A-type and late B stars. Furthermore, the b_i for an object *close* to the Eddington limit are displayed in Fig. 8 with additional energy terms. All the observed lines originate from the energy levels $3s\ ^5S^o$, $3s\ ^3S^o$, $3p\ ^5P$ and $3p\ ^3P$.

Deep in the atmosphere the departure coefficients approach unity as the density increases and collisional processes dominate, enforcing LTE (inner boundary condition). Farther out in

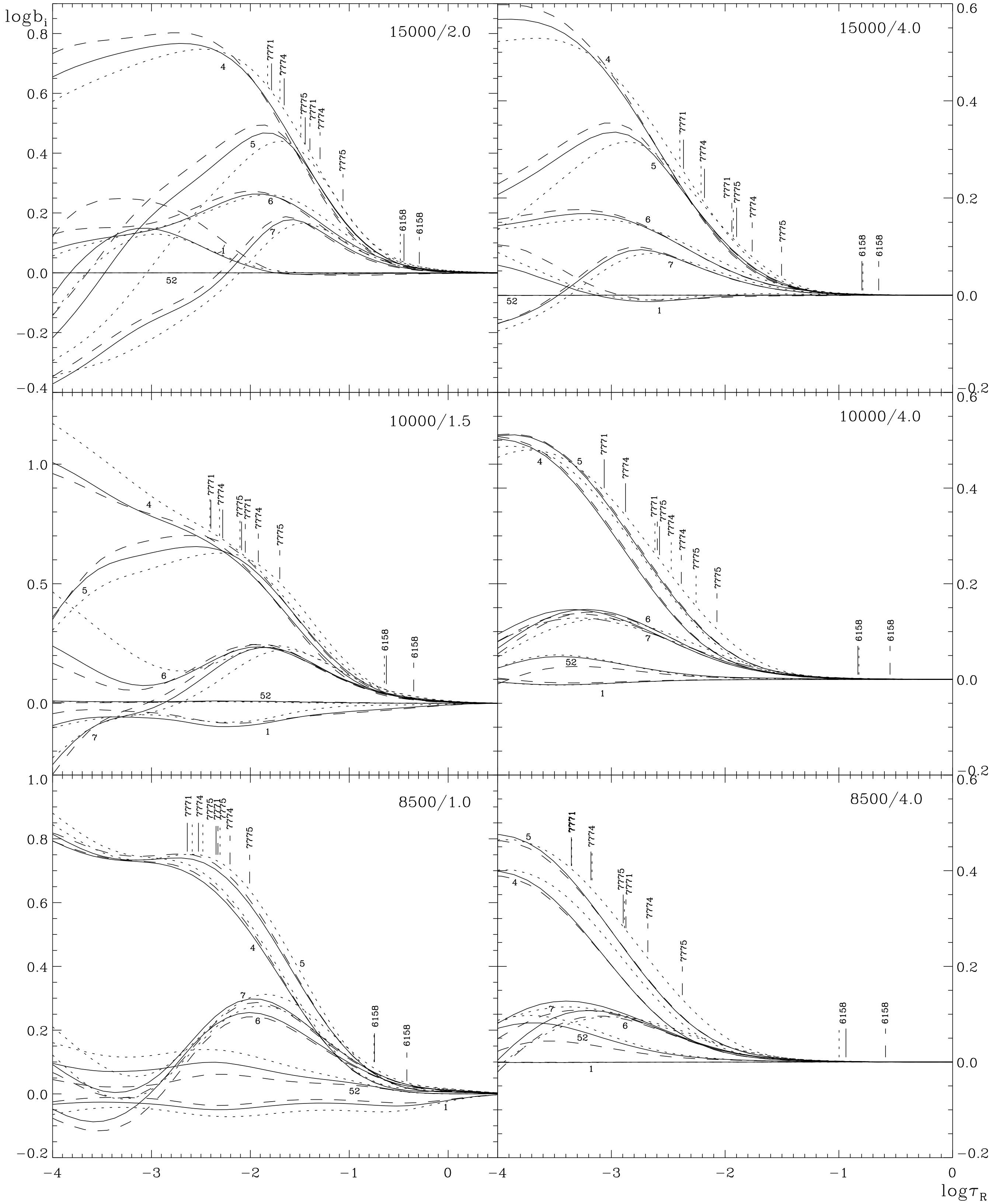

Fig. 7. Departure coefficients b_i of term i as a function of Rosseland optical depth τ_R. Solid line: $\xi = 2\,\mathrm{km\,s^{-1}}$, [O/H] $= 0$, [Fe/H] $= 0$; dotted line: $\xi = 8\,\mathrm{km\,s^{-1}}$, [O/H] $= 0$, [Fe/H] $= 0$; dashed line: $\xi = 2\,\mathrm{km\,s^{-1}}$, [O/H] $= 0$, [Fe/H] $= -0.7$. The formation depths of the line core ($\tau \approx 1$) for several transitions are indicated. Term identifiers – 1: $2p^4\ ^3P$; 4: $3s\ ^5S^o$; 5: $3s\ ^3S^o$; 6: $3p\ ^5P$; 7: $3p\ ^3P$; 52: $2p^3\ ^4S^o$ (O II)

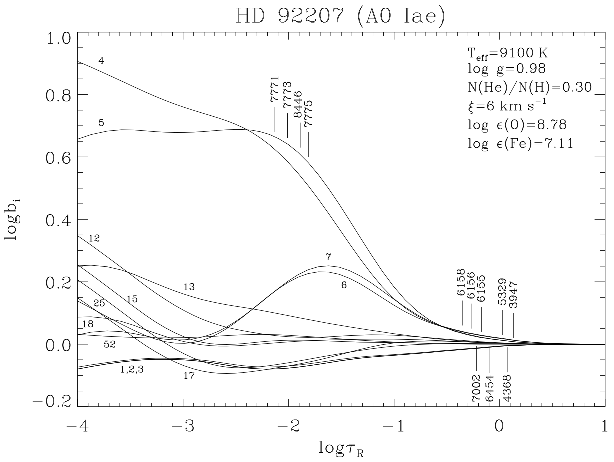

Fig. 8. Departure coefficients b_i as a function of τ_R from the model calculation for the supergiant HD 92207. In addition to those from Fig. 7 the b_i from the following energy terms are also displayed – 2: $2p^4\ ^1D$; 3: $2p^4\ ^1S$; 12: $4p\ ^5P$; 13: $4p\ ^3P$; 15: $5s\ ^5S^o$; 17: $4d\ ^5D^o$; 18: $4d\ ^3D^o$; 25: $5d\ ^5D^o$. The formation depths of the line core ($\tau \approx 1$) for the main diagnostic lines are indicated.

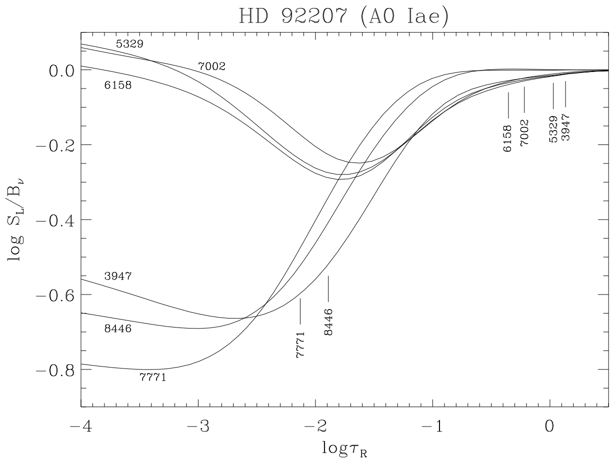

Fig. 9. Ratio of line source function S_L to Planck function B_ν at line centre as a function of τ_R for the supergiant HD 92207. The formation depths of the line cores ($\tau \approx 1$) are indicated

the atmosphere marked deviations from LTE occupations occur, setting in at larger τ_R and being more pronounced in supergiants. Strong overpopulations are found for the metastable level $3s\ ^5S^o$ and for $3s\ ^3S^o$, the lower states for the $\lambda\lambda$ 7771-5 and 8446 transitions, respectively. Overpopulations by a factor of $\sim$4 occur in main sequence stars and 6-16 in supergiants at maximum. This behaviour may be understood in terms of recombinations cascading to lower n via transitions among the levels with quantum numbers (n, $\ell = n - 1$). The radiative downward rates feed the 3s level populations both in the triplet and the quintet spin system. Electron collisions are ineffective in depopulating the metastable $3s\ ^5S^o$ state and the $3s\ ^3S^o$ level. Moreover, the latter energy level also gains metastable character as the net radiative rate to the O I ground state turns out to be essentially zero. However, the two 3s levels are close energetically and can be coupled collisionally at higher densities despite the small collision strength of this (octupole) transition. Thus their departure coefficients behave similarly. The other level populations show much smaller deviations from LTE, less than a factor of 2 even in the supergiants. The 3p levels – the lower levels of the observed weak O I lines – show a moderate overpopulation due to being part of the recombination cascade mentioned above and the strong radiative coupling with the 3s levels. Collisions couple these two levels in the same manner as for the 3s levels at a larger collision strength. In general, accounting for the detailed collision cross sections is essential to determine the non-LTE corrections quantitatively as the lines in the visible and IR are strongly influenced by the collisional processes even in supergiants. Finally, the ground states of O I/O II and the first two excited singlet levels coupled with the O I ground state via strong collision rates deviate only marginally from LTE. This has to be checked for non-LTE atmospheric models where the hydrogen non-LTE departures (negligible here) are expected to be forced upon oxygen via charge exchange. The qualitative behaviour of the b_i for the HD 92207 model is similar to the (10000/1.5) calculation with non-LTE effects setting in deeper in the atmosphere and the departures being more pronounced.

We have just discussed the importance of recombination cascades for the strengthening of the observed oxygen lines. A problem in this context might arise from insufficient collisional coupling of the highest energy levels treated explicitly in our statistical equilibrium calculations with the continuum. As a test we increased the coupling of these levels to the continuum by a factor of 10^3. The populations of the lower levels of the observed lines change by less than 2% with negligible effects on the calculated equivalent widths.

The formation depths of the line core at $\tau \approx 1$ for the strongest lines in the near-infrared and the visible are also indicated in Fig. 7. All other weak lines in the visible are formed even deeper in the atmosphere than λ 6158 (cf. also Fig. 8). The extent of the non-LTE abundance corrections presented in Fig. 5 can be qualitatively deduced from the b_i-diagrams and the behaviour of the line source function S_L as shown exemplary in Fig. 9. A reduction of the metal content in the atmospheric model and the microturbulence affect the departure coefficients only moderately.

The ratio of the line source function to the Planck function

$$\frac{S_L}{B_\nu} = \frac{\exp(h\nu_{ij}/kT) - 1}{n_i g_j / n_j g_i - 1} \tag{4}$$

for an early A-type supergiant model (HD 92207, see Sect. 4) is displayed in Fig. 9, h being the Planck constant, ν_{ij} the transition frequency, k the Boltzmann constant, T the temperature, n the occupation numbers and g the statistical weights of the lower/upper level i/j. The behaviour of S_L/B_ν is qualitatively the same for the supergiant models in our parameter range. Deviations of S_L from B_ν set in deeper in the atmosphere with increasing T_{eff} and decreasing $\log g$. For the near-infrared lines

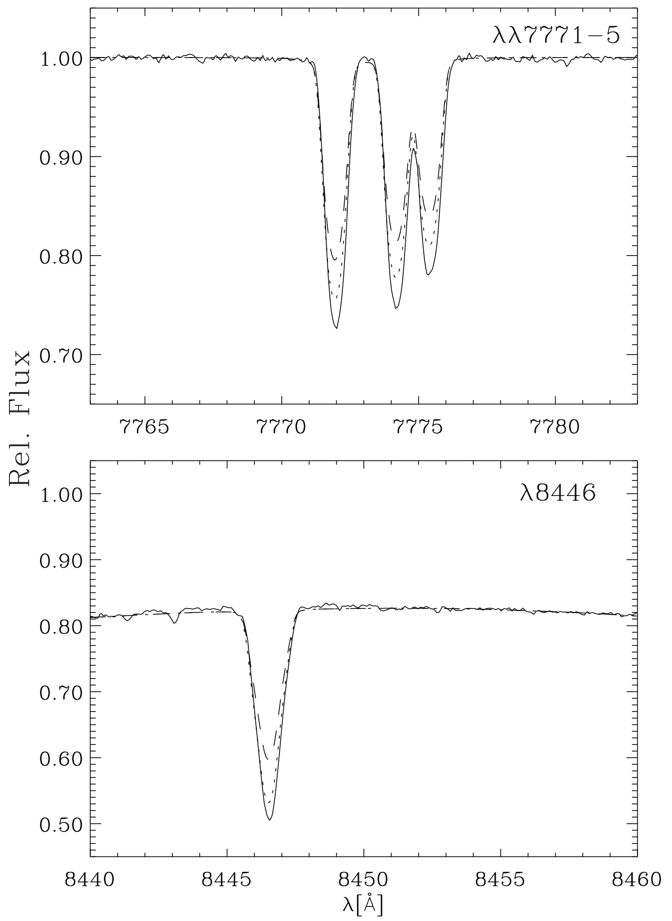

Fig. 10. The importance of collisional cross sections: theoretical line profiles from different atomic models for $\log\varepsilon(\mathrm{O})$=8.59 (as derived in Sect. 4.2) are compared with those observed for Vega (full line). Dotted: collision strengths from Bhatia & Kastner (1995) for most of the transitions between energy levels with $n \leq 3$ adopted; dashed: Van Regemorter (1962) and Allen (1973) approximation (Ω=1 for the latter) for these transitions assumed.

a marked reduction of the line centre intensity is expected due to photon escape (see e.g. Mihalas (1978), Ch. 11-2). This also affects the lines in the visible. Again, variations of microturbulence and metallicity result in only moderate changes as tests have shown. In the main sequence models the non-LTE effects on the line source function are dramatically reduced, deviating from S_L/B_ν=1 only in the outer formation region of the strong near-infrared lines.

A simple approximation to the behaviour of the source functions of the strong near-infrared lines is given by the classical two-level atom. The S_L from the detailed calculation and the simple model resemble each other throughout the line formation region.

Additionally, the ratio of non-LTE to LTE line opacities

$$\frac{\chi_\mathrm{L}}{\chi^*_\mathrm{L}} = b_i \frac{1 - n_j g_i / n_i g_j}{1 - \exp(-h\nu_{ij}/kT)} \tag{5}$$

is found to mainly follow the departure coefficients of the lower levels of the transitions. Thus especially for the strong near-infrared lines a marked increase in the line opacity as compared to LTE is expected. The lines are strengthened enormously due to the (pseudo-)metastability of the lower levels.

3.3. The strong near-infrared lines

Fig. 7 also offers some indication for the reasons for our failure to reproduce the observed strong near-infrared lines. In contrast to the weak lines they are tracers for the physical structure of the stellar atmosphere over a considerable part of its geometrical extent. However, at optical depths $\log\tau_\mathrm{R} \lesssim -1$ non-LTE effects on the model structure of Ib supergiants become more and more important as found by Przybilla (1997). This is the case at even larger τ_R in the atmospheres of the more luminous supergiants. Furthermore, spherical extension of the atmosphere and outflow velocity fields present at the base of the stellar wind of the supergiants will alter the conditions for the line formation significantly. A reinvestigation will shed light on these points as improved model atmospheres become available.

Weaknesses in our O I model atom (especially in the collision rates) might also be present. These may be investigated most easily in main sequence stars where the atmospheric structure is sufficiently well described by the standard assumptions of being plane-parallel, homogeneous, stationary and of being in hydrostatic and radiative equilibrium. In Fig. 10 the results from model calculations with two sets of collisional data are compared with the observed near-infrared lines of Vega. Obviously a significant improvement can be achieved by avoiding widely used approximation formulae for the collisional processes. Therefore the collisional data of Bhatia & Kastner (1995) is used for the rest of our work. Unfortunately, detailed data on collisions are scarce and there is no possibility at present to check whether the remaining differences between theory and observation result from this deficiency or whether alternative explanations can be found (as discussed below).

In anticipation of the spectra analysed in the next section, we discuss our theoretical results for $\lambda\lambda$ 7771-5 in comparison with the observations for the main sequence star Vega and the two supergiants η Leo and HD 92207 in order to show what can be achieved within our approach. The observed profiles for this extremely strong triplet (W_λ larger than those of the strongest Balmer lines in supergiants) are displayed in Fig. 11 together with results from our computations in non-LTE and LTE, see the figure caption for details.

The observed profiles for $\lambda\lambda$ 7771-5 cannot be exactly reproduced with the abundances determined from the weak lines, neither in non-LTE nor in LTE. They indicate a higher oxygen abundance. The absorption coefficient at line centre is increased in non-LTE in addition to a depression of the line source function due to photon escape, resulting in much deeper line profiles compared to the LTE profiles for the same oxygen abundance. Only in the wings do they approach the values given by LTE. But the equivalent widths derived for both are too small compared to those observed as the computed pro-

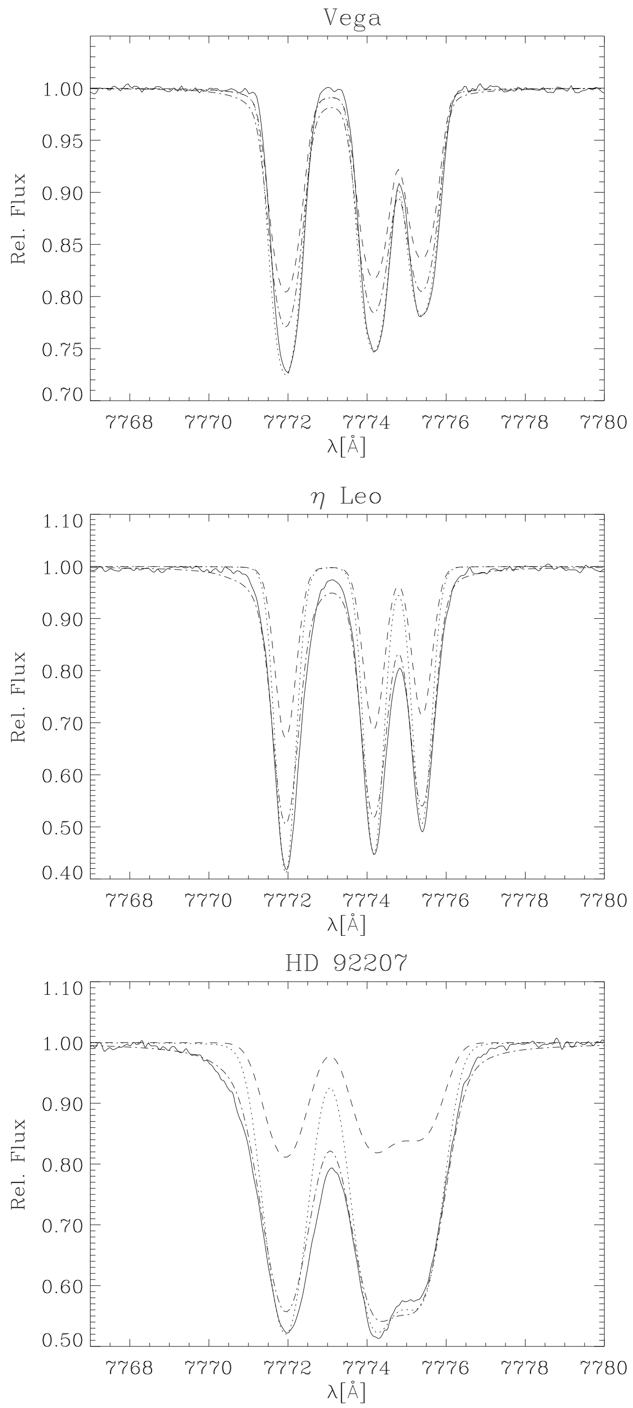

Fig. 11. Comparison of theoretical line profiles for O I $\lambda\lambda$ 7771-5 with those observed for Vega, η Leo and HD 92207 (full line). Dotted: non-LTE line-formation for $\log\varepsilon(\mathrm{O})$ = 8.87/8.92/9.85 (Vega/η Leo/ HD 92207); dashed: LTE line-formation for the same abundances; dashed-dotted: LTE line-formation for $\log\varepsilon(\mathrm{O})$ = 9.20/10.38/10.96 (W_λ of the observed lines reproduced), cf. Table 3.

files are not broad enough in the case of supergiants. A further LTE computation is also displayed that matches the observed W_λ. In this case the line centre is not deep enough but marked damping wings begin to develop, especially in the supergiants. These are not present in the observations. The situation is similar in O I λ 8446. We conclude that *equivalent-width studies of the strong near-infrared* O I *lines are inadequate for abundance determinations*. While non-LTE line formation for these lines occurs on the flat part of the curve of growth, in LTE the large abundances required imply that the formation takes place on the damping part.

For an accurate representation of the line profiles a number of parameters have to be correctly determined. Varying the projected rotational velocity $v \sin i$ and the (*depth independent*) micro- and macroturbulent velocities (ξ, ζ) for the objects within the range given by Table 2 does not improve the fit significantly. Only changes in the microturbulence parameter alter the equivalent width, variation of the other parameters only results in profile changes. The limits are set by numerous other metallic lines throughout the spectra. Furthermore, our Stark broadening parameters for the lines might be inaccurate but tight limits are set for the case of Vega and consequently the values needed to fit the supergiant line wings can be excluded. Weaknesses in our model atom/atmospheres might be another possibility but no definitive conclusions can be drawn as e.g. a depth dependent microturbulence claimed by other authors will resolve the problem, see Sect. 5 for details.

3.4. Comparison with other studies

Several other studies on non-LTE effects for neutral oxygen have been carried out in the past. Two of them deal with the general problem rather than concentrate on particular details so that a comparison with our results is desirable.

Baschek et al. (1977) discuss an O I model consisting of the ground state and the first seven excited energy levels of the quintet spin system plus the continuum. The non-LTE abundance corrections they find are systematically larger than ours. Also the maximum in the line strengths occurs around 10000 K in their calculations in contrast to our results and the available observations (cf. Fig. 5). A closer inspection of their departure coefficients for stellar parameters comparable with ours shows qualitatively similar behaviour; but the non-LTE departures set in deeper in the atmosphere and are also more pronounced. We suppose that their neglect of metal line-blanketing is an important factor in this context as we also find a strengthening of the non-LTE effects when the metallic background opacities are omitted. Note that the modification of the background opacities also results in a change of the atmospheric structure. Due to the absent backwarming effect their models show a reduced local temperature at the line formation region thus explaining the shift of line strength maximum at least qualitatively. As their model atom is quite limited in the energy levels considered and the atomic data also somewhat outdated final conclusions for the discrepancy with our results cannot be drawn. We cannot implement their model atom in DETAIL/SURFACE for further comparison as they used unpublished photoionization cross-sections.

In their O I analysis for Vega they do not find consistent abundances from different lines but they note that the equiva-

Table 2. Basic properties and atmospheric parameters for the test stars

HD	Name	Sp. Type	V (mag)	l (°)	b (°)	$v_{\rm rad}$ (km s^{-1})	$v \sin i$ (km s^{-1})	$T_{\rm eff}$ (K)	$\log g$	ξ (km s^{-1})	$\zeta_{\rm RT}$ (km s^{-1})
172167	α Lyr, Vega	A0 V	0.03	67.44	+19.24	−14	22	9500	3.95	2	0
							±2	±150	±0.1	±0.5	±2
87737	η Leo	A0 Ib	3.52	219.53	+50.75	+3	9	9600	2.00	4	12
							±1	±150	±0.15	±1	±2
92207	...	A0 Iae	5.45	286.29	−0.26	−9	28	9100	0.98	6	18
							±4	$^{+300}_{-150}$	$^{+0.30}_{-0.15}$	±1	±4

lent widths used in this process might be influenced by unidentified line blends in the moderate resolution spectra dating back to Matsushima & Groth (1960).

A comprehensive non-LTE model for neutral oxygen is presented by Takeda (1992). Again, the derived non-LTE abundance corrections are larger than ours as are the departure coefficients b_i. For some levels the behaviour is not even qualitatively similar to that in our work. Tracing the discrepancies back to their origins is difficult as insufficient details are provided. Line-blanketing is accounted for by older ODFs (Kurucz 1979), therefore the background opacities should be somewhat smaller, resulting in strengthened non-LTE departures. In general, the atomic data and even the gf values differ. For Vega abundances from the strong O I lines are slightly underestimated in this model (Takeda 1993) when compared to the weak line results, contrary to our findings. This trend increases dramatically in the calculations for the supergiant α Cyg (Takeda 1992). Whether this is due to an overestimation of the non-LTE effects or due to inaccurate stellar parameters cannot be decided here. Furthermore, as above, line blends might be unaccounted for in the equivalent-width determination.

4. Application to observations

4.1. The spectra

As a test and first application of the model atom oxygen abundances for three stars are determined: Vega, η Leo and HD 92207. High S/N and high resolution spectra are used in this process.

For η Leo and HD 92207 Echelle spectra using FEROS (Kaufer et al., 1999) at the ESO 1.52m telescope in La Silla were obtained in January 1999. Nearly complete wavelength coverage between 3600 and 9200 Å was achieved with a resolving power $R = \lambda/\Delta\lambda \approx 48000$ (with 2.2 pixels per $\Delta\lambda$ resolution element) yielding a S/N of several hundred in V in a 2 and 5 min exposure, respectively. Data reduction was performed using the MIDAS package, as described in the FEROS documentation (http://www.ls.eso.org/lasilla/Telescopes/2p2T/E1p5M/FEROS/docu/Ferosdocu.html). The spectra were normalised by fitting a spline function to continuum points and finally shifted in wavelength to the rest frame using the radial velocity $v_{\rm rad}$ determined from cross-correlation with an appropriate synthetic spectrum.

An Echelle spectrum of Vega was kindly made available by A. Korn with almost complete wavelength coverage between 3900 and 9400 Å. FOCES (Pfeiffer et al. 1998) at the Calar Alto 2.2m telescope was used in June 1999 to obtain three exposures of 4 s and 2×10 s, respectively. The spectra were reduced in the standard way using the routines described by Pfeiffer et al. (1998). After merging of the single spectra and rectification a S/N of ~750 near H_α was measured at $R \approx 40000$ (2 pixels per $\Delta\lambda$ resolution element).

In general, the observations are of high quality with few spectral regions corrupted by CCD defects. As the data were obtained only as an addendum to the main observing program, no additional spectra of a fast rotator are available at the correct airmass to remove the telluric features properly.

4.2. Abundance analysis

The basic properties and atmospheric parameters of the test stars are summarised in Table 2. Information on the basic properties are taken from the Bright Star Catalogue (Hoffleit 1982). Atmospheric parameters for Vega are adopted from Castelli & Kurucz (1993) except for $v \sin i$ which we take from our analysis (still compatible with their value). For the two supergiants atmospheric parameters are determined prior to the oxygen abundance analysis applying the model atmosphere method developed by Venn (1995b) for galactic A-type supergiants, discussed in detail therein. In brief, $T_{\rm eff}$ and $\log g$ are derived simultaneously by finding the ionization equilibrium of Mg I/II using a non-LTE model atom as comprehensive as the one presented here (Przybilla et al. 2000) and by fitting the wings of the higher Balmer lines (typically from H_γ upwards) which are still formed in photospheric regions in contrast to the wind affected H_α and H_β features. For Vega this method leads to the same parameters as derived by Castelli & Kurucz (1993) by comparing observed and computed energy distributions and Balmer profiles. The microturbulent velocity ξ is determined from LTE spectrum synthesis for a large ensemble of Fe II, Ti II and Cr II lines by demanding that there is no relation between abundance and line strength. Rotational velocities $v \sin i$ and macroturbulence $\zeta_{\rm RT}$ in the radial-tangential model are derived from spectrum synthesis as both broadening mechanisms alter the line profile in different ways (Gray 1992). Error estimates for the stellar parameters of the test stars are also given in Table 2.

The results of the abundance analysis for oxygen are summarised in Table 3 which gives the wavelength, multiplet number, lower excitation potential and the adopted gf value for the observed lines (all from Wiese et al. (1996); multiplet num-

Table 3. Abundance analysis for oxygen in the test stars

				α Lyr			η Leo			HD 92207		
λ (Å)	Mult.	χ (eV)	$\log gf$	W_λ(mÅ)	$\log \varepsilon_{\rm NLTE}$	$\Delta \log \varepsilon$	W_λ(mÅ)	$\log \varepsilon_{\rm NLTE}$	$\Delta \log \varepsilon$	W_λ(mÅ)	$\log \varepsilon_{\rm NLTE}$	$\Delta \log \varepsilon$
3947.29	3	9.15	−2.10	S(25)	8.59/8.59[a]	−0.02	35	8.68	−0.04	34	8.80	−0.17
3947.48			−2.24									
3947.59			−2.47									
4368.19	5	9.52	−2.67	S	8.62/8.58	−0.02	34	8.75	−0.11	S	8.73	−0.27
4368.24			−1.96									
4368.26			−2.19									
4654.12	18	10.74	−2.16	...	...	...	12	8.83	−0.05	...	...	...
4654.56			−1.93									
4655.36			−1.79	...	...	...	...	...	...	...	...	...
4772.45	16	10.74	−1.92	S(14)	8.57/8.57	−0.02	14	8.80	−0.04	...	...	...
4772.91			−1.70									
4773.75			−1.55				10	8.68	−0.03			
4967.38	14	10.74	−1.63	24	8.56/8.56	−0.03	47	8.78	−0.07	34	8.79	−0.17
4967.88			−1.41									
4968.79			−1.26									
5329.10	12	10.74	−1.24	59	8.54/8.54	−0.03	50	8.78	−0.11	67	8.77	−0.18
5329.68			−1.02									
5330.73			−0.87				39	8.78	−0.11			
6046.23	22	10.99	−1.76	S	8.64/8.64	−0.02	S	8.83	−0.09	S	8.92	−0.25
6046.44			−1.54									
6046.49			−2.24									
6155.96	10	10.74	−1.36	78	8.61/8.59	−0.03	120	8.80	−0.14	183	8.69	−0.30
6155.97			−1.01									
6155.99			−1.12									
6156.74			−1.49									
6156.76			−0.90									
6156.78			−0.69									
6158.15			−1.84	59	8.62/8.59	−0.05	89	8.80	−0.17			
6158.17			−1.00									
6158.19			−0.41									
6453.60	9	10.74	−1.29	S	8.63/8.60	−0.02	38	8.77	−0.09	S	8.88	−0.26
6454.44			−1.07									
6455.98			−0.92	Blend	...	...	Blend	...	...	Blend	...	...
7001.90	21	10.99	−1.49	S	8.56/8.55	−0.03	S	8.80	−0.15	S	8.63	−0.30
7001.92			−1.01									
7002.17			−2.66									
7002.20			−1.49									
7002.23			−0.74									
7002.25			−1.36									
7771.94	1	9.15	0.37	244	*8.85*/8.56	*−0.30*	509	*8.85*	*−1.50*	2022	*9.85*	*−1.11*
7774.17			0.22	424	*8.88*/8.59	*−0.35*	859	*8.97*	*−1.42*			
7775.39			0.00									
8446.25	4	9.52	−0.46	S(423)	*8.83*/8.61	*−0.69*	S(724)	*8.73*	*−1.70*	S(840)	*8.37*	*−2.19*
8446.36			0.24									
8446.76			0.01									
9260.81	8	10.74	−0.24	Blend	...	...	...	...	...	...	...	...
9260.85			0.11									
9260.94			0.00									
9262.58			−0.37	Blend	...	...	...	...	...	...	...	...
9262.67			0.22									
9262.78			0.43									
9265.83			−0.72	S	*8.80*/8.65	*−0.36*	...	...	...	...	...	...
9265.93			0.13									
9266.01			0.71									
Mean[b]					8.59/8.59	8.62		8.78	8.87		8.78	9.01
σ[b]					0.03/0.03	0.04		0.05	0.08		0.08	0.09

[a]: second entry for a depth-dependent microturbulence, see Sect. 5; [b]: omitting results displayed in italics; the mean and the standard deviation in the column of $\Delta \log \varepsilon$ give the corresponding LTE values

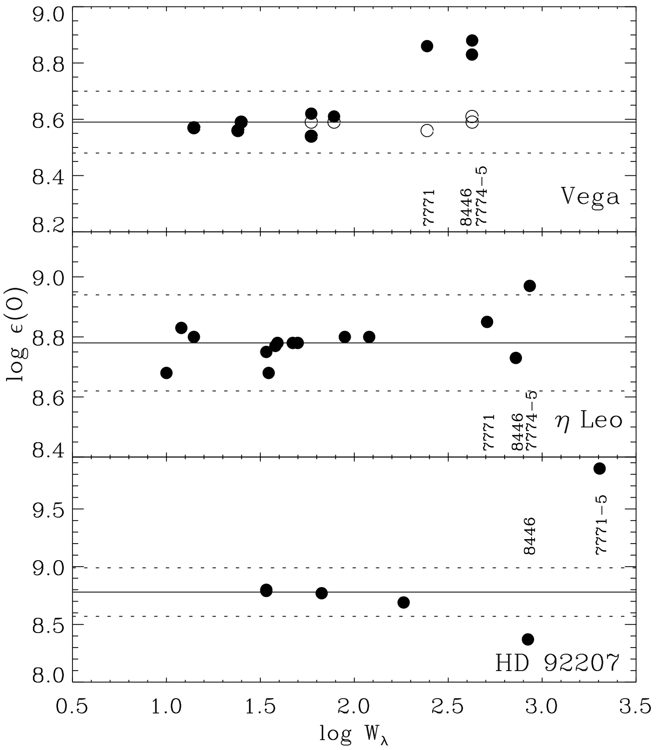

Fig. 12. Non-LTE oxygen abundances from unblended spectral lines for the three test stars are plotted against their equivalent widths (in mÅ). Open circles (for Vega): depth-dependent microturbulence from Gigas (1986) applied, see Sect. 5. Solid line: mean oxygen abundance according to Table 3; dashed lines: error estimates for the mean abundance (1 σ deviations + systematic errors)

Table 4. Accuracy of gf values

Accuracy	Multiplet
±3%	1, 8
±10%	3, 4, 5, 10, 21
±20%	9, 12, 14, 16, 18, 22

bering according to Moore 1976) and the measured equivalent widths, derived abundances $\log\varepsilon$ and non-LTE abundance corrections $\Delta\log\varepsilon$ for the different stars. Blended lines are marked by "S" as long as an analysis via spectrum synthesis is still feasible and for lines originating in the hydrogen line wings the equivalent widths are measured against the local continuum (W_λ in parentheses). Non-LTE and LTE mean values and the line-to-line scatter (σ) from the lines in the visible are also given, the near-infrared lines are omitted for reasons discussed below. For Vega non-LTE abundances for a model with a depth-dependent microturbulence (Gigas 1986, see Sect. 5 for details) are also displayed. Note that the abundances are derived from the detailed spectrum synthesis results and not from an equivalent-width study. We deviate from this general procedure for the near-infrared lines. The LTE abundances and therefore the non-LTE abundance corrections are determined by reproducing the observed equivalent widths as fitting the observed profiles proves to be impossible in LTE. The non-LTE abundances from the individual (unblended) lines of the test stars are plotted versus their equivalent widths in Fig. 12, clearly demonstrating the remarkably small scatter in the line-to-line abundances. In particular, the application of a depth-dependent microturbulence in Vega results in perfect agreement of oxygen abundances derived from the weak and strong lines.

In Figs. 13 to 15 theoretical line profiles for the derived mean non-LTE oxygen abundance are compared with the observations; excellent agreement is found for the lines in the visible. Other elements are included for the spectrum synthesis in LTE in order to disentangle line blends. As some of the oxygen lines are formed in the wings of H I lines, profiles for hydrogen are calculated on the basis of non-LTE level populations. The O I abundances for the test stars are:

Vega	$\log(\mathrm{O/H}) + 12 = 8.59 \pm 0.03 \pm 0.08$ (10/14)
η Leo	$\log(\mathrm{O/H}) + 12 = 8.78 \pm 0.05 \pm 0.11$ (13)
HD 92207	$\log(\mathrm{O/H}) + 12 = 8.78 \pm 0.08 \pm 0.13$ (8)

We list the values obtained from the non-LTE analysis together with uncertainties from the line-to-line scatter and systematic errors (cf. Sect. 2.3); the number of analysed lines is given in parentheses. Non-LTE shifts the derived oxygen abundances systematically to lower values and the line-to-line scatter is slightly reduced in comparison to LTE.

Vega shows an oxygen deficiency of ∼0.3 dex. This is slightly less than its general underabundance in the heavier elements by typically ∼0.5 dex (solar abundances adopted from Grevesse et al. (1996), but see Reetz (1998) for a critical reexamination of the solar oxygen abundance). We find negligible non-LTE corrections for the weak lines in this main sequence star. The quality of the line fit to the strong near-infrared lines is drastically improved by applying a variable microturbulence in the line formation as found by Gigas (1986), while the weak lines are quite insensitive, cf. Sect. 5.

In the case of η Leo the oxygen abundance is marginally below the solar value. Only small ($\lesssim 0.15$ dex) non-LTE abundance corrections apply for the weak lines. On the other hand, huge corrections occur in the strong lines. The line profiles can not be reproduced accurately as an unidentified mechanism broadens the line wings (also present in the wings of strong lines from other elements). Nevertheless, the line depths are predicted quite correctly by adopting the oxygen abundance from the weak lines. Generally, we derive an approximately solar metallicity for this star from the LTE elemental abundance analysis.

For HD 92207 we find an oxygen abundance similar to η Leo with pronounced non-LTE abundance corrections; from the LTE spectrum synthesis we obtain [Fe/H]∼ -0.4 dex. Some regions in the spectrum of this star are still of too low S/N to analyse several of the weakest oxygen lines. The strong O I lines in the infrared are definitely affected by the wind outflow velocity field observed for this star, showing asymmetrical profiles with blueward shifted absorption, as are the strong lines of other elements.

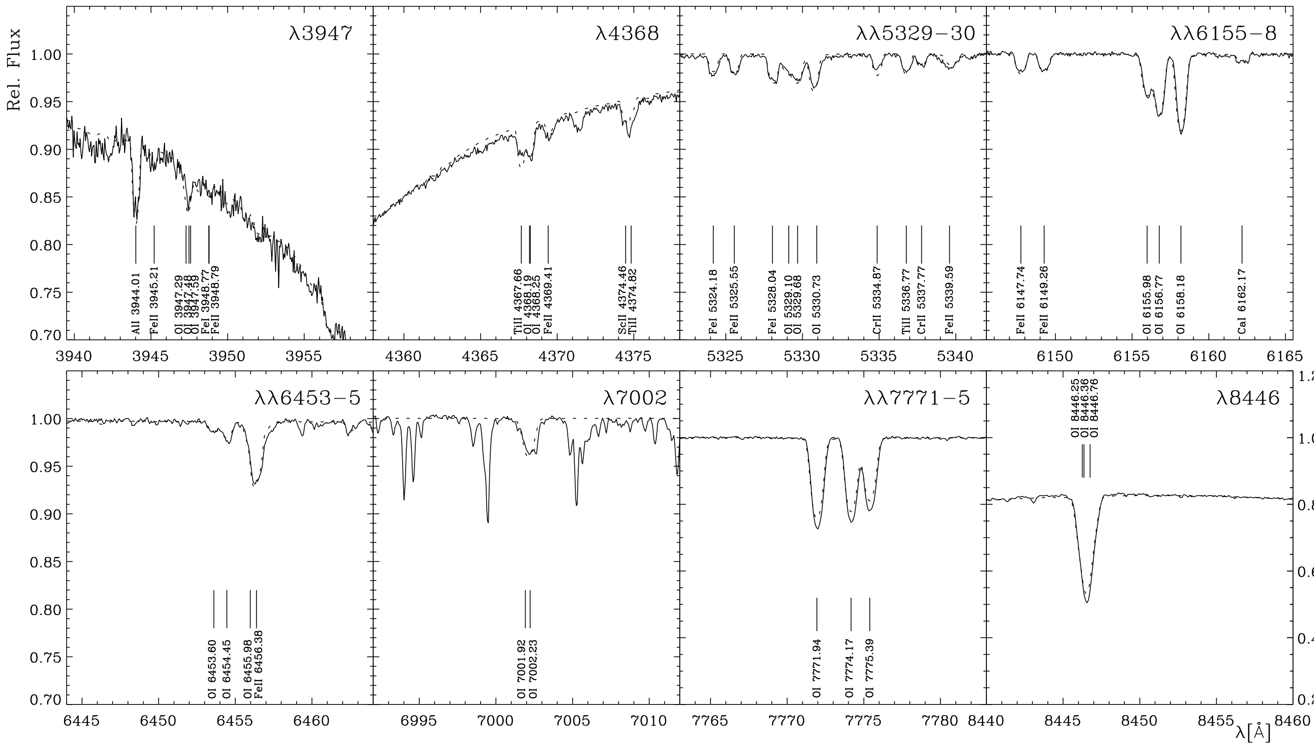

Fig. 13. Observed (solid) and computed (dotted) line profiles for O I in Vega. Displayed is our best fit for the mean oxygen abundance from Tab. 3 along with synthetic line profiles for several other elements calculated in LTE. O I $\lambda\lambda$ 3947, 4368 and 8446 are formed in the wings of hydrogen lines (non-LTE calculation) which define the local continuum. Numerous sharp telluric lines contaminate the red part of the spectrum. Note that the scale of the ordinate for $\lambda\lambda$ 7771-5 and 8446 differs from the other figures (axis labelling at the lower right).

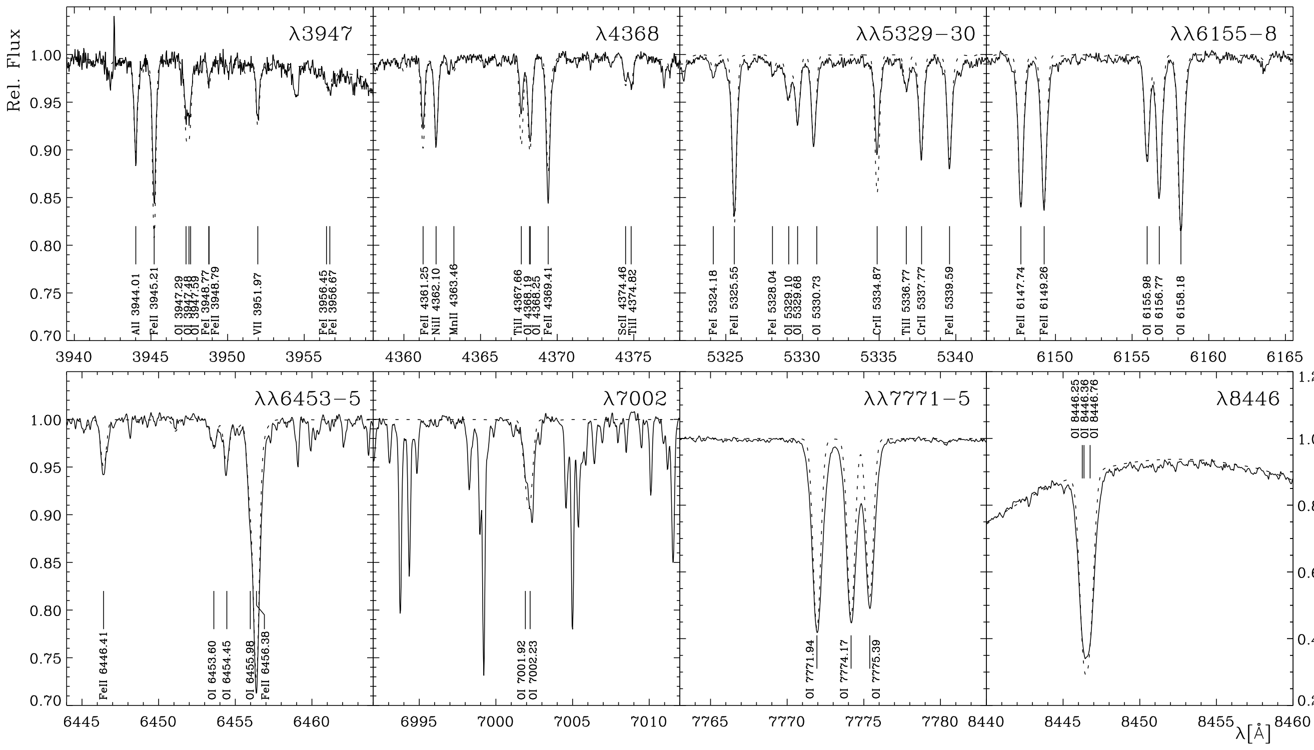

Fig. 14. Same as Fig. 13 for η Leo.

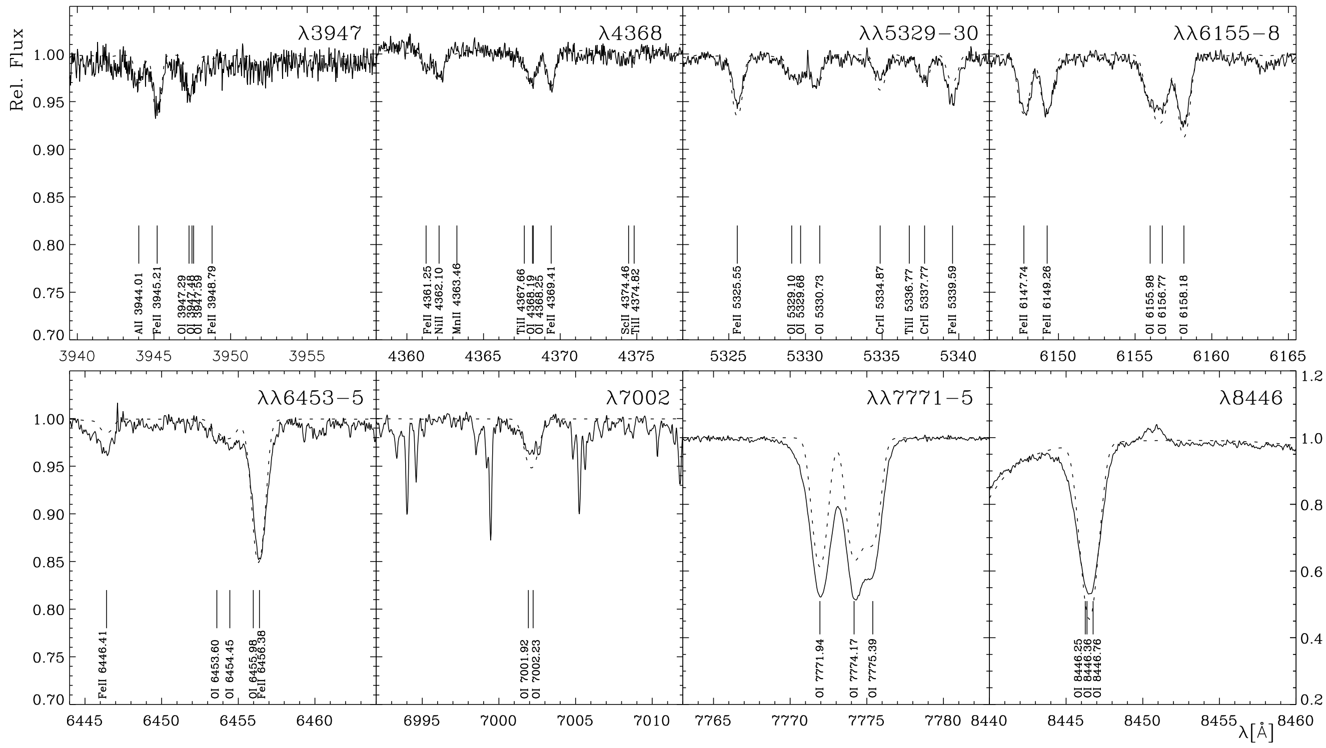

Fig. 15. Same as Fig. 13 for HD 92207. Note that for O I λ 4368 the synthetic spectrum has been shifted to account for the locally enhanced continuum due to incoherent electron scattering in the wing of H_γ (see McCarthy et al. (1997) for a discussion of this effect).

Table 5. Comparison of oxygen abundances for α Lyr and η Leo

Source	$\log\varepsilon_{\rm LTE}$(O)	$\log\varepsilon_{\rm NLTE}$(O)
	α Lyr	
This work	8.62 ± 0.04 (10)	8.59 ± 0.03 (10/14)
Takeda (1993)	8.76 ± 0.06 (5)	~ 8.6 (11)
Venn & Lambert (1990)	8.74 (1)	...
Lambert et al. (1982)	8.82 ± 0.12 (4)	...
	η Leo	
This Work	8.87 ± 0.08 (13)	8.78 ± 0.05 (13)
Takeda & Takada-Hidai (1998)	9.02 (1)	8.70 (1)
Venn (1995a)	8.97 ± 0.05 (6)	...
Lambert et al. (1988)	9.07	...
Wolf (1971)	8.74 ± 0.67 (3)	...

listed are the abundances with errors from the line-to-line scatter (number of lines analysed in parenthesis)

4.3. Comparison with other analyses

In the following our results for Vega and η Leo are compared with those of other recent analyses (cf. Table 5) To our knowledge abundances for the extreme supergiant HD 92207 are determined for the first time.

Vega For this star Takeda (1993) derives an oxygen abundance of $\log\varepsilon$(O)$\sim$8.6 from a non-LTE analysis of 11 O I lines with equivalent widths similar to those from Table 3. The scatter in the abundances from individual lines is larger than ours. Remarkable are the comparatively large non-LTE abundance corrections that he finds – typically two to three times as large as ours, even for the weak lines, cf. Sect. 3.4 for details. His LTE abundance from the weak lines of 8.76 ± 0.06 (5 lines) results partly from using $\log gf$-values $\sim$$0.1 - 0.15$ dex smaller than our OP data. Some of the discrepancy is also related to the different background opacities used (Kurucz, 1979 vs. Kurucz, 1992); his stellar parameters for Vega are almost identical with ours: $T_{\rm eff} = 9500$ K and $\log g = 4.0$ at [Fe/H]~ -0.6 dex.

Venn & Lambert (1990) find an O I abundance of 8.74 from a LTE analysis of $\lambda\lambda$ 6155-8 for the stellar parameters (9650/4.0) and values of $\log gf$ similar to ours. However, their equivalent widths differ by 25% from our measurements.

In the LTE study of Lambert et al. (1982) an abundance of $8.82{\pm}0.12$ is derived from 4 weak O I lines being inconsistent with our findings. Their gf values and their equivalent-width measurements are similar to ours. But they use a model atmosphere with solar elemental composition at $T_{\rm eff} = 9650$ K and $\log g = 4.0$ thus compensating the higher temperatures by increasing the oxygen abundance.

η Leo Takeda & Takada-Hidai (1998) find an oxygen abundance of 8.70 from a non-LTE study of the O I triplet $\lambda\lambda$ 6155-8 in the spectrum of η Leo; they give a comparatively large non-LTE abundance correction of $\Delta\log\varepsilon = -0.32$. Both their non-LTE and their LTE value are just about consistent with our results. The discrepancy can be traced to their stellar parame-

ters ($T_{\rm eff}$=10200 K, $\log g$=1.9) – which would also result in a higher LTE oxygen abundance within our approximation – and to their O I non-LTE model, cf. Sect. 3.4.

Venn (1995a) gives an O I abundance of 8.97 ± 0.05 from a LTE study for stellar parameters (9700/2.0). Comparing our LTE results for the analysed lines ($\lambda\lambda$ 6155-8, 6453-4) with hers gives excellent agreement. In that work non-LTE effects are estimated to result in abundances ~0.2 dex lower, adopting the results of Baschek et al. (1977).

The LTE study of Lambert et al. (1988) finds $[\mathrm{O/H}] = +0.20$ from $\lambda\lambda$ 6155-8 for the stellar parameters (10500/2.00). An appropriate reduction of their $T_{\rm eff}$ would bring their O I abundance into better accordance with ours.

Wolf (1971) derives $[\mathrm{O/H}] = -0.13 \pm 0.67$ from three oxygen lines in an early LTE study on the basis of an unblanketed model atmosphere for the parameters $T_{\rm eff}$=10400 K and $\log g$=2.05 with a depth dependent ξ of 2…10 km s^{-1}. Given the large scatter in the line-to-line abundances, the deviations from our modern gf values (~1 dex in one triplet) and the differences in some of the measured equivalent widths the similarity of his results with our findings is coincidental.

Where not mentioned explicitly, the equivalent widths measured in the studies above agree well with ours and the gf values used are almost identical. The higher effective temperatures adopted by Takeda & Takada-Hidai (1998) and Lambert et al. (1988) can most likely be traced back to differences in the line blanketing (Kurucz 1979) for the model atmospheres.

5. The impact of velocity fields on the line formation

As we have shown in the previous sections, abundances determined from the strong near-infrared lines are not entirely consistent with the results from the weak lines in the visible. The fitting of line profiles for the near-infrared lines in supergiants and to a smaller degree in the main sequence star Vega still poses a problem. There has been some indication that the problems might not result from a possible weakness in our O I non-LTE model atom but from the inadequacy of the standard assumptions in the model atmosphere description. In particular, plane-parallel geometry, stationarity, the assumption of LTE and hydrostatic equilibrium have to be questioned for the atmospheric models of supergiants and deviations from these will become noticeable in the strong lines first as they are formed over a large part of the geometrical extent of the stellar atmosphere. Limitations of the available codes mean that we can only address the influence of velocity fields on the line formation, but as we will see, significant progress can be achieved by taking them into account.

5.1. Microturbulence

Microturbulence has been introduced as a parameter to bring model calculations into better agreement with observation. The concept of some additional non-thermal line-broadening is not out of the question physically despite the lack of a comprehensive theoretical explanation for it at present. In the following we investigate its impact on our line formation calculations.

First, a rather technical question has to be addressed. McErlean et al. (1998) include microturbulence explicitly in the statistical equilibrium calculations (with DETAIL) for helium in OB stars and find significantly different profiles as compared to the standard procedure of including microturbulence only in the final step of the spectrum synthesis (with SURFACE) for microturbulent velocities in excess of 10 km s^{-1}. In the OB-type supergiants thermal velocities $v_{\rm th} = \sqrt{2kT/m}$ (k being the Boltzmann constant, T the temperature and m the mass of the ionic species) for helium are of the same order as the microturbulent velocities (~10 km s^{-1}). Given the larger mass of the oxygen atom and the lower temperatures this ratio becomes approximately 1:3 ($v_{\rm th}$:ξ) in A-type supergiants. A pronounced effect should therefore be expected for the statistical equilibrium calculations from Eq. 1. We find *no* profile changes for oxygen as the level populations are only marginally affected. Still, the classical effects of adopting a microturbulent velocity apply in the final spectrum synthesis.

This unexpected finding is related to the behaviour of the occupation numbers n_i throughout the line formation region for the energy levels involved . The n_i/N (N being the total particle density) for the terms $3\mathrm{s}\ ^5\mathrm{S^o}$, $3\mathrm{s}\ ^3\mathrm{S^o}$, $3\mathrm{p}\ ^5\mathrm{P}$ and $3\mathrm{p}\ ^3\mathrm{P}$ are nearly constant. Thus the line opacity remains almost constant as an increased microturbulence pushes the formation depth of the line centre deeper into the atmosphere but simultaneously broadens the frequency bandwidth for absorption. Only for cases where the occupation numbers vary strongly on small geometrical scales do the effects of microturbulence as proposed by McErlean et al. (1998) come into operation.

More recent studies for stellar abundances (among others e.g. Venn 1995b) favour the application of a *depth independent* microturbulent velocity to bring abundances from weak and strong lines into agreement. The bulk of the metallic lines in the spectra of our test stars can be satisfactorily reproduced by this assumption, the remaining discrepancies attributed to inaccuracies in the gf values and to unaccounted non-LTE effects. For the strong O I lines these explanations can be quite probably excluded as discussed above.

We investigate what can be achieved if a *depth dependent* microturbulence is invoked. For Vega, a depth dependent ξ is derived by Gigas (1986) from a non-LTE study of Fe I/II lines varying from $0-3.5$ km s^{-1} through the atmosphere (bottom to top). The abundances derived from the individual lines are displayed in Table 3. A remarkably small scatter around the mean oxygen abundance is found for *all* lines. In Fig. 16 the resulting line profiles for the mean value are presented for $\lambda\lambda$ 6155-8, 7771-5, 8446 and 9260-5 in comparison with the profiles for a depth independent ξ of 2 km s^{-1} for the same elemental abundance. Lines weaker than $\lambda\lambda$ 6155-8 are virtually insensitive to the change in the microturbulence parameter. For $\lambda\lambda$ 6155-8 a slightly better concordance for the single components is achieved while the fit for the stronger lines is significantly im-

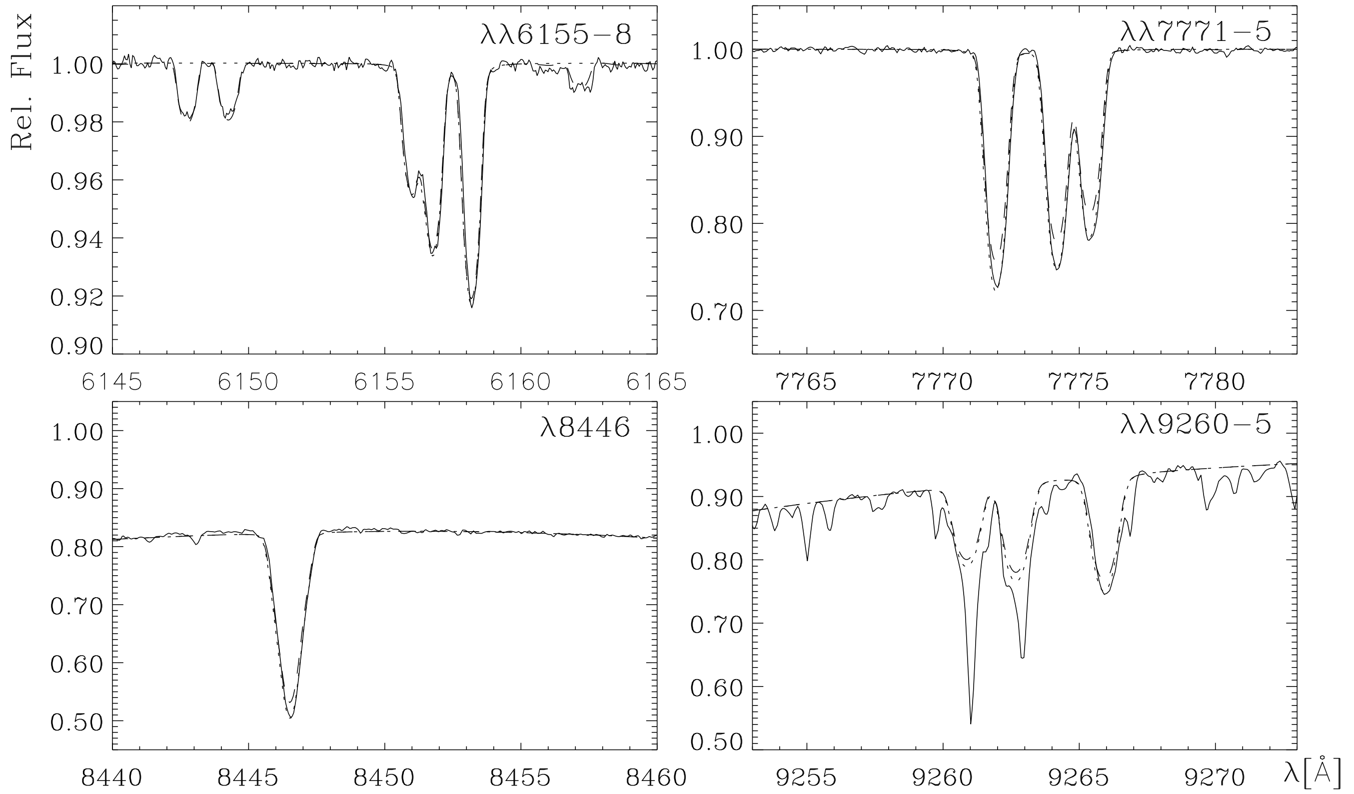

Fig. 16. The impact of a depth dependent microturbulence in the case of Vega. Displayed are the observed profiles (full line) of the stronger O I lines and theoretical profiles for a constant microturbulence of ξ=2 km s^{-1} as in the last section (dashed) and for a depth dependent ξ (0…3.5 km s^{-1} throughout the atmosphere, dotted) as derived by Gigas (1986). The weaker lines remain virtually unaffected, cf. Fig. 13 for profile fits.

proved as can be expected from their position on the curve of growth.

Also in the case of supergiants a significant improvement can be achieved, with the necessary microturbulent velocities not exceeding the speed of sound. But, by adopting a depth dependent microturbulence the quality of the (LTE) fits for lines from other elements is worsened and different velocity fields for various elements are required, as found in other studies (e.g. Rosendhal 1970; Aydin 1972). A definite statement cannot be made in this context as non-LTE calculations especially for the iron group elements (the microturbulence indicators) are not available, although work on this is in progress.

5.2. Wind outflow velocity fields

An alternative explanation for the large ($\sim$ speed of sound) microturbulent velocities observed in supergiants is provided by Kudritzki (1992), cf. also Lamers & Achmad (1994) for the case of A-type supergiants. The subsonic outflow velocity field at the base of the stellar wind in supergiants will strengthen lines saturated just in their line cores even for the moderate mass-loss observed in the latter types. Desaturation of the lines due to the Doppler shifts experienced by the moving medium is the driving mechanism for the strengthening of the spectral features. For higher mass-loss rates even weak lines can be affected. This might be interpreted as a large "microturbulent" velocity in the hydrostatic approach. A macroscopic velocity field will also result in: a blue-shift of the central wavelength (increasing with equivalent width) and an asymmetry in the line profile with extra absorption in the blue wing. A-type supergiants offer an opportunity to verify these predictions due to the comparatively small rotational velocities observed for these stars. At earlier spectral types the effects of the wind on the weak lines are likely to be masked by the higher $v \sin i$.

For the galactic supergiant HD 92207 the following parameters are used for fitting the H_α/H_β/H_γ features with the SPH code (Kudritzki et al. 1999):

$T_{\rm eff}$ = 9800 K	$\dot{M}$ = 1.6 10^{-6} M$_\odot$/yr
$\log g$ = 1.02	v_∞ = 235 km s^{-1}
Y = 0.22	β = 1.0
$R_\star$ = 210 R$_\odot$	

(with Y being the ratio of He to H by number, $R_\star$ the stellar radius, $\dot{M}$ the mass loss rate, v_∞ the terminal velocity and β the velocity law coefficient).

Based on this SPH model atmosphere we investigate the impact of the implementation of a (β-type) velocity field in the non-LTE radiative transfer calculations on the computed line profiles. In Fig. 17 the results are displayed for the O I lines $\lambda\lambda$ 7771-5 and 6155-8 for $\log \varepsilon$(O)=8.78. For comparison, the line profiles resulting from the hydrostatic approach with an

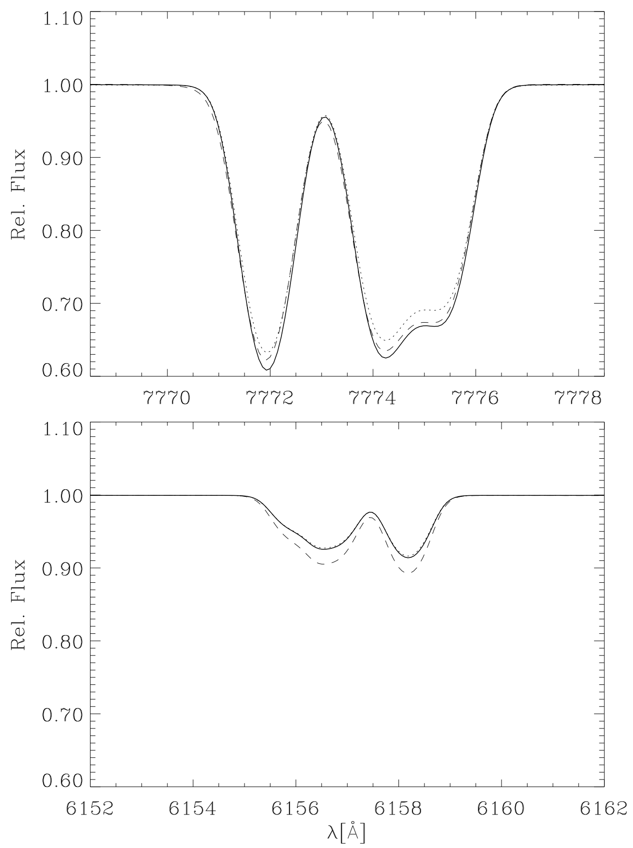

Fig. 17. The impact of a hydrodynamic outflow velocity field on the line formation. Displayed are theoretical line profiles of O I $\lambda\lambda$ 7771-5 (top) and 6155-8 (bottom) calculated for the stellar parameters of HD 92207 in the hydrostatic approach (ATLAS9 model, full line) and broadened according to the observations. The other two profiles are based on a hydrodynamic model (SPH) with the velocity field accounted for in the line formation calculation (dashed) and with the velocity field neglected (dotted).

ATLAS9 atmosphere are also included. Despite the differences in the stellar parameters used (needed to compensate the absence of metal line blanketing in the SPH model) the profiles for the weak lines from the ATLAS9 and the SPH model – neglecting the velocity field – are almost identical. The strong lines on the other hand are weakened due to the lower local densities in the outer atmosphere of the SPH model. Taking the velocity field into account results in the effects described above. Both strong and weak lines strengthen, but only in the strong features do the blueward shift of the line centre and the line profile asymmetry become noticeable. The strengthening of $\lambda\lambda$ 7771-5 is not large enough to explain the strength of the observed feature – it is not even sufficient to reproduce the hydrostatic calculations – and for $\lambda\lambda$ 6155-8 the theory produces lines that are too strong. An explanation for this behaviour might be a too steep velocity gradient. Reducing the slope would diminish the velocities at the formation depth of the weak lines and would also shift the position of the sonic point further out in the atmosphere, thus expanding the formation depth of the strong lines. As the density drops rapidly beyond the sonic point, the medium becomes optically thin at the line frequencies and the feature appears too weak. In addition, the shift of the line centre is too large compared with the observation, also implying a too large value of the local velocity.

Certainly, this topic deserves further attention as it offers the opportunity to study the velocity stratification in detail at the base of the stellar wind. But, due to the large number of parameters involved the theoretical description of the unified model atmospheres has to be refined first. In particular, line blanketing has to be accounted for in the models to give a realistic description of the atmospheric stratification, presently the subject of extensive work at the Universitätssternwarte München.

Finally, a last point concerning supergiants has to be mentioned here. In addition to the macroscopic velocity field the spherical extension of the atmosphere will also strengthen the near-infrared O I lines: the probability for photon escape is increased in the extended atmosphere thus the line source function is further depressed resulting in a stronger spectral feature. It is our hope that by accounting for all these effects we will be able to determine consistent abundances from all O I lines in supergiants with the present model atom.

6. Summary and conclusions

An extensive model atom for non-LTE line formation calculations for neutral oxygen in BA-type stars has been developed, based on the most accurate atomic data presently available. The weak O I lines in the visible prove to be highly reliable abundance indicators at all luminosities while the strong near-infrared lines are tracers for the atmospheric structure. They are of only limited use for deriving accurate abundances in supergiants with present atmospheric models.

We have provided a set of non-LTE abundance corrections for the diagnostic O I lines, applicable over a large range of stellar parameters in BA-type stars. Along the main sequence non-LTE effects on O I are negligible for the weak lines, are gradually increasing with luminosity to reach significant values in Ib supergiants and are essential for the analysis of the most luminous objects close to the Eddington limit where non-LTE corrections in excess of 0.5 dex are predicted in some cases. High accuracy in the determination of oxygen abundances can be achieved, within expected uncertainties of $\sim$0.10/0.15/0.20 dex for high quality observations of main sequence/Ib/Ia objects *including* systematic errors as confirmed by the analysis of our three test stars Vega, η Leo and HD 92207. We have derived the following oxygen abundances:

Vega	$\log(\mathrm{O/H}) + 12 = 8.59 \pm 0.03 \pm 0.08$
η Leo	$\log(\mathrm{O/H}) + 12 = 8.78 \pm 0.05 \pm 0.11$
HD 92207	$\log(\mathrm{O/H}) + 12 = 8.78 \pm 0.08 \pm 0.13$

Our results support the findings of a slight oxygen underabundance for Vega in previous studies. η Leo and HD 92207 turn out to show a slightly less than solar oxygen abundance.

The theoretical interpretation of the strong near-infrared lines still poses some problems as they are formed over a large range in the geometrical extent of the stellar atmosphere. Present atmospheric models fail to describe the actual physical conditions realistically, especially in supergiants. A consistent treatment of non-LTE effects and (non-LTE) line blanketing on the atmospheric structure is still lacking.

Nevertheless, we have shown that – apart from weaknesses within our model atom which we cannot completely exclude as for the majority of the highly important collisional processes only approximate data are available – certain simple assumptions are sufficient to remove most of the discrepancies between observation and theory. Significant improvement can be achieved by invoking a depth dependent microturbulence parameter, having a large impact on the saturated lines but leaving the weak lines almost unaffected. For Vega perfect consistency for all oxygen lines has been achieved by this. The technical point of the inclusion of microturbulence for additional line broadening in the statistical equilibrium calculations has also been investigated. In contrast to studies for other elements, no effect on line profiles and equivalent widths is found in our O I non-LTE computations which can be explained from the interplay between occupation numbers and formation depths for varying microturbulence.

The observed asymmetric line profiles with blueward shifted extra absorption in extreme supergiants demand consideration of the hydrodynamic velocity field (and spherical extension) for the spectrum synthesis computations. Some improvement in removing the discrepancies between theory and observation can be achieved by accounting for the macroscopic velocity field where, in the hydrostatic case, the depth dependent microturbulence has to be invoked. This insight cannot be gained from the simple equivalent-width studies performed in the past; detailed line profile analyses have to be carried out. The strong metal lines in the A-type supergiants offer a unique opportunity to study the velocity field at the base of the stellar wind.

A final statement on the line formation of the strong near-infrared O I lines cannot be presented here as from the theoretical standpoint some effort has to be made to describe the physical conditions in a supergiant's atmosphere realistically. But with this study we hope to focus the attention on the importance of non-LTE effects, micro- *and* macroscopic velocity fields for the line formation.

Acknowledgements. We are grateful to A. Kaufer for his help with obtaining some of the spectra at La Silla and to S. Tubbesing for his help with the data reduction. Our work benefits much from the beautiful spectrum of Vega provided by A. Korn. We express our thanks to our referee, Dr. D. Kiselman, for many useful suggestions and we would also like to acknowledge helpful discussions with J. Puls. RPK likes to thank the director and staff of Steward Observatory, Tucson, for their hospitality and support during his sabbatical. Funding through the MPIA, Garching, is gratefully acknowledged (NP).

References

Allen C., 1973, Astrophysical Quantities, 3rd edn., Athlone Press, London
Arnaud M., Rothenflug R., 1985, A&AS, 60, 425
Aydin C., 1972, A&A, 19, 359
Baschek B., Scholz M., Sedlmayr E., 1977, A&A, 55, 375
Bhatia A.K., Kastner S.O., 1995, ApJS, 96, 325
Butler K., Giddings J., 1985, Newsletter on Analysis of Astronomical Spectra No. 9, University of London
Butler K., Zeippen C.J., 1990, A&A, 234, 569
Butler K., Zeippen C.J., 1991, J. Phys. IV, Colloq. C1, 141
Butler K., Zeippen C.J., 2000, J. Phys. B, in preparation
Castelli F., Kurucz R.L., 1993, In: Dworetsky M.M., Castelli F., Faraggiana R. (eds.), IAU Colloq. 138, Peculiar versus Normal Phenomena in A-Type and Related Stars, San Francisco: ASP
Cavallo R.M., Pilachowski C.A., Rebolo R., 1997, PASP, 109, 226
Chung S., Lin C.C., Lee E.T.P., 1993, Phys. Rev. A, 47, 3867
Cowley C., 1971, Observatory, 91, 139
Faraggiana R., Gerbaldi M., van 't Veer C., Floquet M., 1988, A&A, 201, 259
Giddings J.R., 1981, PhD Thesis, University of London
Gigas D., 1986, A&A, 165, 170
Gray D.F., 1992, The observation and analysis of stellar photospheres, 2nd edition, Cambridge University Press
Grevesse N., Noels A., Sauval A.J., 1996, In: Holt S.S., Sonneborn G. (eds.), Cosmic Abundances, San Francisco: ASP
Griem H.R., 1974, Spectral Line Broadening by Plasmas, Academic Press, New York and London
Henry R.J., 1970, ApJ, 161, 1153
Hoffleit D., 1982, The Bright Star Catalogue, New Haven: Yale Univ. Obs.
Hofsäß D., 1970, Diplomarbeit, Universität Hamburg
Humphreys R.M., McElroy D.B., 1984, ApJ, 284, 565
Johnson H.R., Milkey R.W., Ramsey L.W., 1974, ApJ, 187, 147
Kaufer A., Stahl O., Tubbesing S., et al., 1999, The ESO Messenger 95
Kiselman D., 1993, A&A, 275, 269
Kudritzki R.P., 1973, A&A, 28, 103
Kudritzki R.P., 1988, In: Chmielewski Y., Lanz T. (eds.), 18th Advanced Course of the Swiss Society of Astrophysics and Astronomy (Saas-Fee Courses): Radiation in Moving Gaseous Media, Geneva Observatory
Kudritzki R.P., 1992, A&A, 266, 395
Kudritzki R.P., 1998, In: Aparicio A., Herrero A., Sánchez F. (eds.), Proc. VIIIth Canary Islands Winter School: Stellar Astrophysics for the Local Group, Cambridge University Press
Kudritzki R.P., Puls J., Lennon D.J., et al., 1999, A&A, 350, 970
Kurucz R.L., 1979, ApJS, 40, 1
Kurucz R.L., 1991, In: Crivellari L. et al. (eds.), Stellar Atmospheres: Beyond Classical Models, NATO ASI Ser. C-152, p. 441
Kurucz R.L., 1992, Rev. Mex. Astrofis., 23, 45
Lambert D.L., Roby S.W., Bell R.A., 1982, ApJ, 254, 663
Lambert D.L., Hinkle K.H., Luck R.E., 1988, ApJ, 333, 917
Lamers H.J.G.L.M., Achmad L., 1994, A&A, 291, 856
Matsushima S., Groth H.G., 1960, Z. Astrophys., 49, 126
McCarthy J.K., Kudritzki R.P., Lennon D.J., et al., 1997, ApJ, 482, 757
McErlean N.D., Lennon D.J., Dufton P.L., 1998, A&A, 329, 613
Mihalas D., 1978, Stellar Atmospheres (2nd ed.), W.H. Freeman and Company, San Francisco

Moore C.E., 1976, Selected Tables of Atomic Spectra, Atomic Energy Levels and Multiplet Tables O I, PB-253 231, U.S. Department of Commerce, Washington
Peach G., 1967, Mem. R. Astron. Soc., 61, 13
Pfeiffer M.J., Frank C., Baumüller D., et al., 1998, A&AS, 130, 381
Przybilla N., 1997, Diplomarbeit, Ludwig Maximilians Universität, München
Przybilla N., Butler K., Becker S.R., et al., 1999, In: Walsh J.R., Rosa M.R. (eds.), Proc. ESO Workshop on Chemical Evolution from Zero to High Redshift, Springer Verlag
Przybilla N., Butler K., Becker S., Kudritzki R.P., 2000, in preparation
Puls J., 1991, A&A, 248, 581
Reetz J., 1998, PhD Thesis, Ludwig Maximilians Universität, München
Rosendhal J.D., 1970, ApJ, 160, 627
Rybicki G.B., Hummer D.G., 1991, A&A, 245, 171
Santolaya-Rey A.E., Puls J., Herrero A., 1997, A&A, 323, 488
Sawada T., Ganas P.S., 1973, Phys. Rev. A, 7, 617
Seaton M.J., 1962, In: Atomic and Molecular Processes, Academic Press, New York
Seaton M.J., Yu Y., Mihalas D., Pradhan A.K., 1994, MNRAS 266, 805
Simon T., Landsman W.B., 1997, ApJ, 483, 435
Skillman E.D.., 1998, In: Aparicio A., Herrero A., Sánchez F. (eds.), Proc. VIIIth Canary Islands Winter School: Stellar Astrophysics for the Local Group, Cambridge University Press
Takeda Y., 1992, PASJ, 44, 309
Takeda Y., 1993, In: Dworetsky M.M., Castelli F., Faraggiana R. (eds.), Peculiar Versus Normal Phenomena in A-Type and Related Stars, San Francisco: ASP
Takeda Y., Takada-Hidai M., 1998, PASJ, 50, 629
Tayal S.S., 1992, J. Phys. B, 25, 2639
Tayal S.S., Henry R.J.W., 1989, Phys. Rev. A, 39, 4531
Thompson W.R., Shah M.B., Gilbody H.B., 1995, J. Phys. B, 28, 1321
Van Regemorter H., 1962, ApJ, 136, 906
Venn K.A., 1995a, ApJ, 449, 839
Venn K.A., 1995b, ApJS, 99, 659
Venn K.A., Lambert D.L., 1990, ApJ, 363, 234
Wang S., McConkey J.W., 1992, J. Phys. B, 25, 5461
Wiese W.L., Fuhr J.R., Deters T.M., 1996, J. Phys. & Chem. Ref. Data, Mon. 7
Wolf B., 1971, A&A, 10, 383